

# The Dynamic Age of Centaurus A

Jean A. Eilek<sup>1,2</sup>

<sup>1</sup> New Mexico Institute of Mining and Technology, Socorro, New Mexico, 87801, USA

<sup>2</sup> Adjunct astronomer, National Radio Astronomy Observatory, P. O. Box O, Socorro, NM 87801 USA.

E-mail: jeilek@aoc.nrao.edu

## Abstract.

In this paper I present dynamic models of the radio source Centaurus A, and critique possible models of in situ particle reacceleration (ISR) within the radio lobes. The radio and  $\gamma$ -ray data require neither homogeneous plasma nor quasi-equipartition between plasma and magnetic field; inhomogeneous models containing both high-field and low-field regions are equally likely. Cen A cannot be as young as the radiative lifetimes of its relativistic electrons, which range from a few to several tens of Myr. Two classes of dynamic models – flow driven and magnetically driven – are consistent with current observations; each requires Cen A to be on the order of a Gyr old. Thus, ongoing ISR must be occurring within the radio source. Alfvén-wave ISR is probably occurring throughout the source, and may be responsible for maintaining the  $\gamma$ -ray-loud electrons. It is likely to be supplemented by shock or reconnection ISR which maintains the radio-loud electrons in high-field regions.

Submitted to: *New J. Phys.*

## 1. Introduction

The full story of the radio galaxy Centaurus A is still not known, despite much careful study over the years. Cen A is of course worth study for its own sake, but it also provides a nearby, well-documented example from which we can understand the dynamic evolution of other, similar radio galaxies. In this paper I focus on two unresolved questions related to Cen A's large-scale radio lobes.

The first question is the age of Cen A. To answer this we need to understand the physical state of its radio lobes. So-called Fanaroff-Riley Type II ("FR II") radio galaxies are well understood: a collimated, supersonic jet develops a terminal shock where it impacts the ambient medium. The shock is apparent as an outer hot spot, and jet plasma which has been through the shock is left behind as a cocoon. Ram pressure drives the growth of the source, as the end of the jet advances into the ambient medium. However, Cen A is not an FR II, but a Fanaroff-Riley Type I ("FR I"; implicitly defined these days as any radio galaxy that is not an FR II). No robust models exist yet for the dynamics and development of FRI sources. The inner jets in some FRI's have been modelled as turbulent, entraining flows, but that model does not address the variety

of FRI morphologies, nor does it describe the history and growth of such a source. More work is needed before we can understand the dynamics of FRI sources.

The second question is how Cen A keeps shining long past the radiative lifetimes of its radio-loud and  $\gamma$ -ray loud electrons. In this paper I discuss three alternative dynamical models which may describe Cen A. All of these models require the source to be quite old, with an age between several hundred Myr to more than a Gyr. This age range is much longer than the electrons' radiative lifetimes, which range from a few to a few tens of Myr. It follows that the radiative lifetimes are not a good indicator of the age of the source; in situ reacceleration (ISR) must be ongoing within the large radio lobes. Thus, Cen A provides a nearby case study of ISR in radio galaxies.

To address these questions, I begin in Section 2 by describing the setting and collecting important facts to be used in the analysis. In Section 3 I review observational constraints on plasma and magnetic field within the outer lobes. I argue that inhomogeneous models, containing both strong and weak fields, are physically likely and consistent with the data. In Section 4 I show that the short radiative lifetimes require ISR; models fail which try to grow the source so quickly. In Section 5 I present three alternative dynamic models – buoyant, magnetic tower and flow-driven – each of which requires the source age to be on the order of a Gyr. The buoyant model does not fare well when compared to the data but both the flow-driven and magnetically-driven models seem consistent with current observations. In Section 6 I critique competing ISR models. I speculate that Alfvén-wave ISR is operating throughout the lobes and probably maintains the  $\gamma$ -ray-loud electrons, while the radio-loud electrons are energized by shock or reconnection ISR in high-field regions within the source. Finally in Section 7 I summarize my arguments and discuss what this exercise reveals about the astrophysics of Cen A. I relegate necessary but tedious details to the Appendices.

## 2. Useful facts and numbers

Cen A's parent galaxy, NGC 5128, is the dominant galaxy in a small group of galaxies. It hosts a massive black hole which is currently active, and must have been so for most of the past Gyr. The plasma driven out by the active galactic nucleus (AGN) has created the large radio galaxy which we see today.

### 2.1. Large scales: the outer radio lobes

Cen A is perhaps best known by its large-scale, double-lobed radio source, extending  $\sim 8.2^\circ$  on the sky, or 540 kpc end-to-end in projection (using 3.8 Mpc distance; Harris *et al* 2010), as shown in Figure 1. These outer lobes have been called giant lobes in the literature, but they are not unusually large compared to other double-lobed radio galaxies. I therefore drop the "giant" and just call them "outer lobes" or "radio lobes".

The outer lobes have been detected in radio from 5 MHz to 5 GHz (*e.g.*, Alvarez *et al* 2000), and recent WMAP images detect the outer lobes up to 60 GHz (Hardcastle 2009, "H09"). While generally similar, the radio structures of the north and south outer lobes differ in detail. The north lobe is straighter (extending  $\sim 4.5^\circ \sim 300$  kpc in projection), while the south lobe broadens and bends. The outer lobes are also clearly detected as extended  $\gamma$ -ray sources (Abdo *et al* 2010, "A10"), interpreted as inverse Compton scattering (ICS) of photons from the cosmic microwave background (CMB).

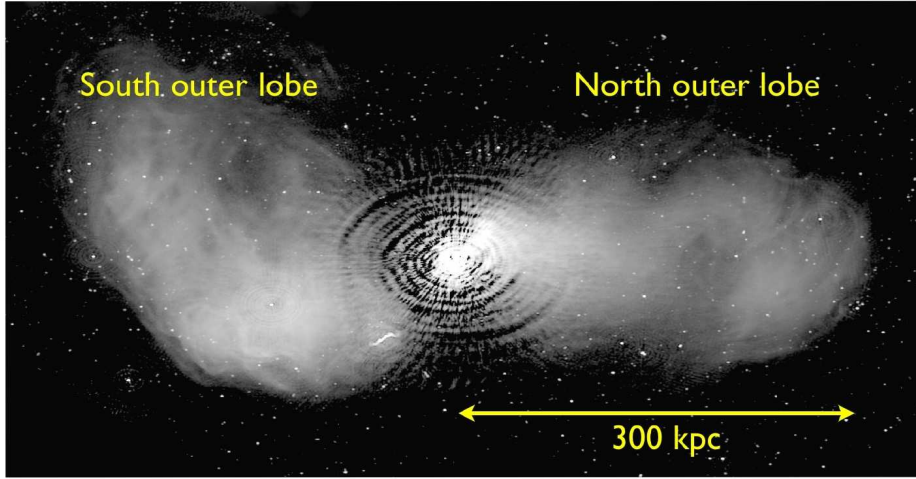


**Figure 1.** The large-scale structure of Centaurus A, displayed with north to the right. Neither lobe shows any sign of limb brightening; the volume of each lobe appears to be filled with localized, radio-bright filaments and loops. Elliptical rings in the center of this image are not physical, but are part of the interferometer response (to the very strong central source) which has not been fully removed from the image. The inner lobes sit within and are obscured by these artifacts. Mosaiced 1.4-GHz image using ATCA and Parkes data,  $60'' \times 40''$  resolution (data are publicly available on the NASA Extragalactic Database; see also Feain *et al* 2011).

When numbers are needed I illustrate with the north lobe. The angle  $\theta$  by which the north lobe deviates from the sky plane is unknown; I keep  $\mu = \cos \theta$  as a parameter. The width of the north lobe is also uncertain. Although relatively narrow at high radio frequencies (*e.g.*, Junkes *et al* 1993), recent data suggest that it is broader when seen in low radio frequencies (PAPER data at 148 MHz from Stefan *et al* 2013; MWA data at 118 MHz from McKinley *et al* 2013) and even broader when seen at  $\gamma$ -rays (recent *Fermi*-LAT data from Yang *et al* 2012, “Y12”). Based on these data I treat the north lobe as a cylinder, with length  $\sim 300/\mu$  kpc, and diameter  $\sim 180$  kpc. The geometry of the south lobe is less clear; it may be a broader ovoid, or it may be a longer structure seen in projection.

## 2.2. Small scales: drivers and inner radio structure

In the past few Myr the AGN in NGC 5128 has created a bipolar inner radio lobe structure,  $\sim 15$  kpc end to end (in projection). Estimates of the power currently being supplied by the AGN to each side of the radio source range from  $\sim 0.7 \times 10^{43}$  erg/s to  $\sim 2 \times 10^{43}$  erg/s (Croston *et al* 2009, Wykes *et al* 2013, Neff *et al* 2014).

Although Cen A is typical of the general radio galaxy population on large and small scales – both showing bipolar radio lobes – it is atypical on the transition scales ( $\sim 20$ – $50$  kpc). No radio jets have been detected connecting the inner and outer radio lobes. A previous suggestion of a weak jet extending to NE (Morganti *et al* 1999) is not supported by newer data (Neff *et al* 2014).

### 2.3. Conditions in the ambient medium

The large angular size of Cen A makes direct X-ray measurements of the surrounding intergalactic medium (IGM) challenging. On small scales – probably representative of the inner part of the IGM surrounding Cen A – Kraft *et al* (2009) modelled X-rays from a  $\sim 35$ -kpc region surrounding NGC5128 as coming from a sphere with density  $\sim 10^{-3}\text{cm}^{-3}$  and temperature  $\sim 0.35$  keV.

To characterize the IGM on larger scales, we must look for analogs among other galaxy groups and poor clusters. Cen A sits in a small group of galaxies (Karachentsev *et al* 2007) with gravitating mass  $\lesssim 9 \times 10^{12} M_{\odot}$ . The group is comparable to, but a bit smaller than, other galaxy groups and poor clusters for which good X-ray data is available. The temperature of the IGM has been measured, typically at  $\sim 1$  keV, for quite a few similar galaxy groups (e.g., Finoguenov *et al* 2006, Sun *et al* 2009). When temperature structure can be resolved, the IGM tends to be cooler in the core, rising to  $\gtrsim 1$  keV by  $\sim 100$  kpc. Determining the density of the IGM in faint, irregular galaxy groups is harder. Doe *et al* (1995) studied several poor clusters, a few times more massive than the Cen A cluster but of comparable size. They found the IGM density  $\sim 5 \times 10^{-4} - 3 \times 10^{-3}\text{cm}^{-3}$  inside  $\sim 100$  kpc, falling off  $\propto r^{-1.5}$  at larger radii. Thus it seems likely that the IGM around most of the outer lobes in Cen A is less dense than the estimate from Kraft *et al* (2009) for the inner region of NGC5128, perhaps  $n_{\text{IGM}} \sim 10^{-4}\text{cm}^{-3}$  (see also discussion in O’Sullivan *et al* 2013).

This estimate for the IGM density differs from that of Bouchard *et al* (2007), who searched for HI in 18 galaxies in the Cen A group. They detected HI in some but not all galaxies, and ascribed the non-detections to stripping by the IGM, suggesting  $n_{\text{IGM}} \sim 10^{-3}\text{cm}^{-3}$ . However, following the basic stripping argument of Gunn and Gott (1972) with the galaxy properties assumed by Bouchard *et al*, it is easy to show that a typical galaxy will be stripped by any IGM density  $n_{\text{IGM}} \gtrsim 10^{-4}\text{cm}^{-3}$ .

Putting these results together, I will scale the IGM density around the outer lobes of Cen A to  $10^{-4}\text{cm}^{-3}$ , the temperature to 1 keV, and estimate the IGM pressure as  $p_{\text{IGM}} \sim 3.2(n_{-4}T_{\text{keV}}) \times 10^{-13} \text{ dyn-cm}^{-2}$ . The likely density decay in the IGM between 100 and 300 kpc means  $p_{\text{IGM}}$  is probably a bit higher around the inner part of the radio lobes, and a bit lower around the outer part.

### 3. Conditions within the outer lobes

In order to evaluate models of the outer lobes, we must understand their internal state. Our diagnostics are radio and  $\gamma$ -ray observations. Gamma rays detected by *Fermi*-LAT from the outer lobes of Cen A are a direct probe of highly relativistic electrons in the outer lobes. Electron energies  $\gamma \sim 3.4 \times 10^5 - 2.8 \times 10^6$  are needed to make  $\gamma$ -rays at 100 MeV – 7 GeV by ICS on the CMB.

Radio emission detected from Cen A is a separate, less direct, probe of the plasma and magnetic field in the lobes. Synchrotron emission maps the electron energy to a photon energy,  $\nu_{\text{sy}} = a\gamma^2 B$ , where  $a \simeq 0.3(3/4\pi)(e/m^3c^5)\sin\theta$  (Pacholczyk 1970; noting the maximum of the  $F(x)$  synchrotron kernel is at  $x \sim 0.3$ ). Numerically, with  $\sin\theta \sim 0.5$ , this becomes  $\nu_{\text{sy}} \sim 0.6\gamma^2 B_{\mu\text{G}}$ . Thus, radio emission at 10 MHz comes from electrons with  $\gamma \sim 4.1 \times 10^3/B_{\mu\text{G}}^{1/2}$ ; emission at 5 GHz comes from electrons with  $\gamma \sim 9.1 \times 10^4/B_{\mu\text{G}}^{1/2}$ . This is a key point: for  $\mu\text{G}$  or stronger magnetic fields, the radio emission comes from a different electron population than does the  $\gamma$ -ray emission.

In this section I use the radio and  $\gamma$ -ray data to derive constraints on the plasma and field in the radio lobes. I discuss various B field models, based both in observations and theory, and argue that the magnetic field must vary – on both small and large scales – within the source. I summarize the possible field values and models in Table 3.

### 3.1. Relativistic electrons in the radio lobes

From the observed  $\gamma$ -ray and radio power we can derive the total energy in  $\gamma$ -ray-loud electrons and find a useful estimate of the total energy in radio-loud electrons.

*Gamma-ray loud plasma.* The ICS energy loss rate for an electron at energy  $\gamma$ , sitting in the CMB, depends only on its energy and fundamental parameters,

$$P_{ICS}(\gamma) \simeq \frac{4}{3} c \sigma_T \gamma^2 \frac{B_{CMB}^2}{8\pi} = b_{ICS} \gamma^2 \quad (1)$$

where  $B_{CMB} = (8\pi u_{CMB})^{1/2} \simeq 3.24 \mu\text{G}$ . To find the total ICS luminosity,  $L_{ICS}$ , let the  $\gamma$ -ray-loud electrons have a power-law energy distribution,  $n_{ICS}(\gamma) \propto \gamma^{-t}$ . An electron spectral index  $t \sim 4.2$  will create a  $\gamma$ -ray photon index  $\sim 2.6$  (consistent with the values reported in A10, Y12). These “ICS electrons” have total energy

$$U_{e,ICS} = \int_{\gamma_2} \gamma m c^2 n_{ICS}(\gamma) d\gamma \quad (2)$$

for  $\gamma_2 \sim 3.4 \times 10^5$ . It is straightforward to connect  $U_{e,ICS}$  to the ICS luminosity above 100 MeV,  $L_{ICS} = \int_{\gamma_2} b_{ICS} \gamma^2 n(\gamma) d\gamma$ :

$$U_{e,ICS} \simeq \frac{t-3}{t-2} \frac{m c^2}{b_{ICS} \gamma_2} L_{ICS} \quad (3)$$

To apply this to Cen A, I convert the  $\gamma$ -ray flux from A10 to luminosity  $L_{ICS}$ , using  $t = 4.2$ . The results are given in the first two columns of Table 1.

**Table 1.** The energy in relativistic electrons in the outer lobes of Cen A. ICS derivation assumes electron spectrum  $n_{ICS}(\gamma) \propto \gamma^{-4.2}$  in  $\gamma$ -ray-loud energy range. Synchrotron derivation assumes  $n_{sy}(\gamma) \propto \gamma^{-2.4}$  in radio-loud energy range and observing frequency  $\nu_o = 1.4$  GHz.  $U_{e,sy}(\nu_1)$  assumes  $\nu_1 = 10$  MHz;  $U_{e,sy}(\gamma_1)$  assumes  $\gamma_1 = 10$ . For other values,  $U_{e,sy} \propto \nu_1^{-0.2} \propto \gamma_1^{-0.4}$ .

Region	$L_{ICS}$ (erg s <sup>-1</sup> )	$U_{e,ICS}$ (erg)	$S(\nu_o)$ (Jy)	$U_{e,sy}(\nu_1)$ (erg)	$U_{e,sy}(\gamma_1)$ (erg)
North lobe	$5.6 \times 10^{40}$	$6.6 \times 10^{54}$	166	$1.4 \times 10^{57} B_{\mu G}^{-1.5}$	$1.6 \times 10^{58} B_{\mu G}^{-1.7}$
South lobe	$8.0 \times 10^{40}$	$1.0 \times 10^{55}$	316	$2.7 \times 10^{57} B_{\mu G}^{-1.5}$	$3.0 \times 10^{58} B_{\mu G}^{-1.7}$

*Radio-loud plasma.* Unlike ICS, the synchrotron energy loss rate for an electron at  $\gamma$  depends on the local B field:

$$P_{sy}(\gamma) \simeq \frac{4}{3} c \sigma_T \gamma^2 \frac{B^2}{8\pi} = b_{sy} \gamma^2 B^2 \quad (4)$$

Let the radio-loud electrons also have a power-law energy distribution,  $n_{sy}(\gamma) \propto \gamma^{-s}$  over some energy range  $\gamma_1 \lesssim \gamma \lesssim \gamma_{br}$ , with an index  $s \sim 2.4$  (corresponding to radio spectral index  $\alpha_{rad} \sim 0.7$ , typical of the outer lobe spectrum below a few GHz; Alvarez *et al* 2000, also H09). The total energy in “synchrotron electrons” is

$$U_{e,sy} = \int_{\gamma_1}^{\gamma_{br}} \gamma mc^2 n_{sy}(\gamma) d\gamma \quad (5)$$

Just as for  $\gamma$ -ray-loud electrons, the energy in radio-loud electrons can be connected to the radio power. However, unlike the ICS result in (3), the conversion for radio is subject to uncertainties in the B field and the low-energy cutoff  $\gamma_1$ . It is convenient here write the synchrotron luminosity in terms of the spectrum  $S(\nu)$ , as  $L_{sy} = \int_{\nu_1}^{\nu_{br}} S(\nu) d\nu$ . A bit of algebra connects the energy in radio-loud electrons to the B field:

$$U_{e,sy} = \frac{2}{s-2} \frac{mc^2 a^{1/2}}{b_{sy}} \frac{\nu_o^{(s-1)/2}}{\nu_1^{(s-2)/2}} \frac{S(\nu_o)}{B^{3/2}} \quad (6)$$

Here,  $\nu_o$  is the fiducial (observing) frequency,  $\nu_1 = a\gamma_1^2 B$ , and the B field is assumed to be approximately constant within the radio-loud region.

Equation (6) contains a critical parameter,  $\nu_1 \propto \gamma_1^2$ . The literature contains two different treatments of  $\nu_1$ . (1) Several authors (*e.g.*, Myers and Spangler 1985, also A10) choose a low  $\gamma_1$  based on ISR models. Typical choices are  $\gamma_1 \sim 10-100$  (corresponding to  $\nu_1 \sim 60$  Hz to 6 kHz in a  $\mu$ G B field, well below the limit of terrestrial radio observation). (2) Other authors (*e.g.*, Burbidge 1956, Pacholczyk 1970) choose  $\nu_1$  as the lowest observed radio frequency, which implies a significantly larger  $\gamma_1$ . Because  $U_{e,sy}$  is dominated by the lowest electron energies, this more conservative choice gives lower values for pressure and energy.

To calculate  $U_{e,sy}$ , I use radio fluxes at 1.4 GHz measured by H09 over the same spatial regions in Cen A used by A10 to measure the  $\gamma$ -ray fluxes. I found  $U_{e,sy}$  for  $\nu_1 = 10$  MHz and also for  $\gamma_1 = 10$  (in the spirit of A10, Y12; corresponding to  $\nu_1 = 60B_{\mu G}$  Hz); for other values,  $U_{e,sy} \propto \nu_1^{-0.2} \propto \gamma_1^{-0.4}$ . The results are given in Table 1, where two trends warrant comment. The lower electron energy cutoff ( $\gamma_1 = 10$ ) gives a factor  $\gtrsim 10$  increase in  $U_{e,sy}$ ; this difference is due to the assumption that the power law electron spectrum continues to energies a factor  $\gtrsim 100$  lower than those observed. In addition, comparing  $U_{e,ICS}$  to either  $U_{e,sy}$  value shows that, for  $\mu$ G-level B fields, the bulk of the electron energy is in radio-loud electrons; the energy in ICS-loud electrons is insignificant.

### 3.2. From observations: two useful limits

The radio luminosity can be used to find lower limits on the pressure and on the B field in radio-loud regions.

*Minimum magnetic field.* We begin with the smallest B field compatible with the radio power. Since the plasma is a synchrotron source, there must be a finite magnetic field, but it may be weak,  $p_B \ll p_{rel}$ . In this limit, if the lobes are in pressure balance with the IGM, we know  $p_{rel} \lesssim p_{IGM}$ . To use this limit, we must connect  $U_e \simeq U_{e,sy}$  (from Table 1), to  $p_{rel}$ . This requires two correction factors, neither of which can be predicted *a priori*; they must be constrained from observations or ancillary data, as follows.



(1) The radio-loud plasma may not fully fill the source. I use the observed volume corresponding to the measured  $S(\nu_o)$  and  $L_{ICS}$  values ( $V_{obs} \sim 1.1 \times 10^{71} \text{cm}^3$  for north lobe,  $\sim 0.87 \times 10^{71} \text{cm}^3$  for south lobe; H09, A10), but also allow for a volume filling factor  $\phi$ . Slices taken across the radio image in Figure 1 show that the outer lobes of Cen A are not limb brightened, but approximately center filled. This, plus the fact that few “holes” are seen in the image, suggests that  $0.1 \lesssim \phi \lesssim 1$  describes Cen A. (2) Relativistic baryons may coexist with the radio-loud leptons. This is measured by the “ $k$ ” factor:  $p_{rel} = (1 + k)p_e$ . In a pure lepton plasma,  $k = 0$ ; in galactic cosmic rays,  $k \simeq 100$ . Because the ISR mechanisms (to be discussed in Section 6) will energize baryons as well as leptons, and because baryons do not suffer radiative losses, we might expect  $k \gg 1$  in Cen A. I combine both  $k$  and  $\phi$  in a pressure scaling factor,  $\xi = (1 + k)/\phi$ , and carry  $\xi$  through the calculations. My estimated ranges of  $k$  and  $\phi$  suggest that  $1 \lesssim \xi \lesssim 10^3$  may hold for the outer lobes of Cen A.

With these definitions, the pressure in relativistic particles is  $p_{rel} = \xi U_{e,sy}/3V_{obs}$ . Using  $U_{e,sy}$  values from Table 1,  $p_{IGM}$  from Section 2.3, and arguing  $p_{rel} \lesssim p_{IGM}$ , we find the minimum magnetic field allowed in each of the outer lobes:

$$B_{min}^{sy}(\text{North}) \sim 0.06 \xi^{2/3} \mu\text{G} ; \quad B_{min}^{sy}(\text{South}) \sim 0.10 \xi^{2/3} \mu\text{G} \quad (7)$$

Here, I take  $\nu_1 = 10$  MHz and  $n_4 T_{keV} = 1$  for the IGM; for other values,  $B_{min}^{sy} \propto (\nu_1^{0.2} p_{IGM})^{-2/3} \propto (\gamma_1^{0.4} p_{IGM})^{-2/3}$ . The reader should note that  $B_{min}^{sy}$  is not to be confused with  $B_{min\ p}$ , the field associated with the minimum-pressure condition, which comes next.

*Minimum pressure.* We can also find the lowest pressure (in relativistic particles and B field) compatible with the observed synchrotron power. This standard calculation, described in many sources (*e.g.*, Pacholczyk 1970), is also subject to the uncertainty in the low-energy cutoff of the electron spectrum described in Section 3.1.† Because a higher  $\gamma_1$  gives a lower minimum pressure, I assume  $\nu_1 = 10$  MHz, equivalent to  $\gamma_1 \simeq 4000 B_{\mu\text{G}}^{-1/2}$ . For other values  $B_{min\ p} \propto \nu_1^{-0.057}$  with my choice  $\alpha = 0.7$ . The key input from the data is the volume emissivity of the radio source, which I took from the Parkes 4.75-GHz map of Cen A (Junkes *et al* 1993), kindly provided by N. Junkes. (Calculations using measurements of the 1.4-GHz image in Figure 1 gave similar results). I measured the average surface brightness within four regions which were roughly equivalent to regions 1, 2, 4, 5, used by H09 and A10, and assumed an average line of sight depth  $100' \sim 110 \text{kpc}$ . The results, keeping  $\xi$  as an unknown parameter, are given in Table 2. Two trends deserve comment. We see that  $B_{min\ p} > B_{min}^{sy}$ . This is expected because  $p_{rel} \sim p_B$  in the minimum-pressure model, while  $p_{rel} \gg p_B$  in the minimum-field model. In addition, if  $\xi \gtrsim 50$ , we have  $p_{min\ p} \gtrsim p_{IGM}$ . This suggests that radio emission may come from localized, high-pressure regions within the lobes; I return to this in Section 3.4.

### 3.3. From observations: homogeneous models

Gamma rays produced by ICS are a potentially powerful tool for determining the magnetic field, because ICS luminosity is independent of the B field. Combining  $\gamma$  rays with radio synchrotron can in principle break the  $e$ – $B$  degeneracy and determine

† I follow Pacholczyk (1970) in assuming that  $\nu_1$  is known; other authors, *e.g.*, Myers & Spangler (1985) do the calculation assuming  $\gamma_1$  is known. Because  $\nu_1$  and  $\gamma_1$  are related by the unknown B field, the algebra is different for each case; see Neff *et al* (2014) for details.

**Table 2.** Minimum-pressure values for outer lobes. Calculations assumed  $\alpha = 0.7$  and  $\nu_1 = 10$  MHz; for other values  $B_{min\ p} \propto \nu_1^{-0.057}$ . The scaling factor  $\xi = (1 + k)/\phi$ ;  $k$  is the ratio of relativistic baryons to leptons, and  $\phi$  is the filling factor (Section 3.2).

Region	$F_5\text{ GHz}$ (Jy)	Box area ( $\text{amin}^2$ )	$p_{min\ p}$ ( $\text{dyn cm}^{-2}$ )	$B_{min\ p}$ ( $\mu\text{G}$ )
North outer	30.	$9.2 \times 10^3$	$2.8 \xi^{4/7} \times 10^{-14}$	$0.55 \xi^{2/7}$
North inner	45.	$8.0 \times 10^3$	$3.8 \xi^{4/7} \times 10^{-14}$	$0.64 \xi^{2/7}$
South inner	134.	$2.4 \times 10^4$	$5.1 \xi^{4/7} \times 10^{-14}$	$0.74 \xi^{2/7}$
South outer	84.	$1.4 \times 10^4$	$2.9 \xi^{4/7} \times 10^{-14}$	$0.56 \xi^{2/7}$

B uniquely, *if synchrotron and ICS come from same electron population*. However, as we saw above, in Cen A the ICS and synchrotron emission come from different electron energies; thus further assumptions are necessary.

One approach (A10, Y12) assumes a homogeneous source, with a uniform B field and a single electron population. In this case the electron energy distribution,  $n(\gamma)$ , must be fine-tuned to produce both the radio spectrum (power law at low frequencies, with steepening above a few GHz) and the steeper  $\gamma$ -ray spectrum. Specifically, the electron spectrum must have either two breaks in energy, or one break with a high-energy curvature. Given an assumed  $n(\gamma)$  which satisfies these constraints, it is straightforward to estimate the ratio  $U_{e,sy}/U_{e,ICS}$ , and from that estimate the B field.

A simple example reveals the essence of this calculation (also carried out by A10, Y12). In curve (a) of the left panel of Figure 2 I show a broken power-law  $n(\gamma)$ , representative of the specific  $n(\gamma)$ 's chosen by A10, Y12, but easier analytically. Referring back to (2) and (5), and using the notation of Figure 2, this example gives

$$\frac{U_{e,sy}}{U_{e,ICS}} = \frac{t-2}{s-2} \frac{\gamma_2}{\gamma_{br}} \left( \frac{\gamma_2}{\gamma_1} \right)^{s-2} \quad (8)$$

Once  $\gamma_1, \gamma_{br}$  and  $\gamma_2$  are chosen, equating the ratio  $U_{e,sy}/U_{e,ICS}$  inferred from the data (as in Table 1) to the ratio calculated from (8) determines the B field required throughout the source. The break energies are constrained by observations. The *Fermi*-LAT data require  $\gamma_2 \sim 3.4 \times 10^5$ , and the radio break at 5 GHz requires  $\gamma_{br} \sim 9 \times 10^4 B_{\mu G}^{-1/2}$ . However,  $\gamma_1$  is uncertain, as discussed in Section 3.1. It is therefore useful to carry out this calculation for both high and low  $\gamma_1$  values.

If  $\nu_1 = 10$  MHz, Table 1 gives  $U_{e,sy}/U_{e,ICS} \sim 240 B_{\mu G}^{-3/2}$ . Equating this to the expression in (8) gives  $B \sim 1.4 \mu\text{G}$  in the outer lobes, an electron energy  $U_{e,sy} \sim 1 \times 10^{57}$  erg and a magnetic energy  $\sim 7 \times 10^{57}$  erg. The electron spectrum is truncated at  $\gamma_1 \sim 3500$ , and the system is field-dominated:  $U_B \sim 7 U_{e,sy}$ . Alternatively, if  $\gamma_1 = 10$ , a similar calculation gives about the same field,  $B \sim 1.5 \mu\text{G}$ , but a larger electron energy,  $U_{e,sy} \sim 1.5 \times 10^{58}$  erg. Thus, with this low  $\gamma_1$ , the electron/field balance has reversed. Because of the abundant low-energy electrons, the system is now marginally electron-dominated, with  $U_{e,sy} \sim 2 U_B$ . This recovers the “quasi-equipartition” particle-field balance, similar to results in A10 and Y12.



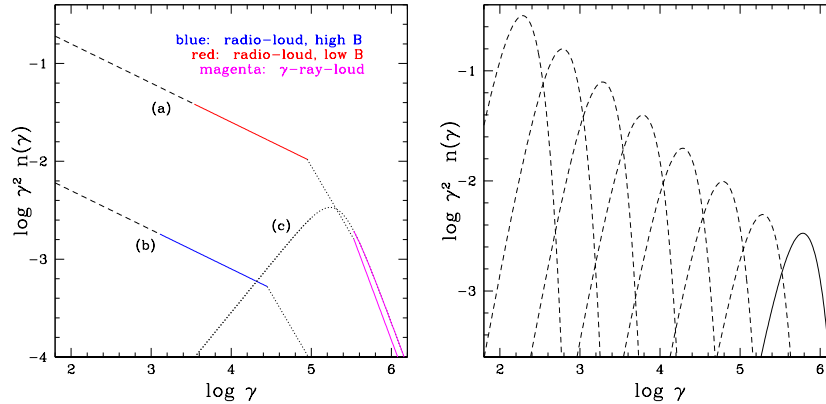


**Figure 2.** Example electron distributions to illustrate discussion in the text. Left: uniform and two-part spectra, as discussed in Sections 3.3 and 3.4. The colored sections of the curves show the regions actually probed by observations; the dotted and dashed lines are not constrained by any current data. The continuous curve (a) describes a homogeneous source with  $B = 1\mu\text{G}$  throughout; it has  $n(\gamma) \propto \gamma^{-2.4}$ ,  $\gamma_1 \lesssim \gamma \lesssim \gamma_{br}$ ;  $n(\gamma) \propto \gamma^{-3.4}$ ,  $\gamma_{br} \lesssim \gamma \lesssim \gamma_2$ ; and  $n(\gamma) \propto \gamma^{-4.2}$ ,  $\gamma \gtrsim \gamma_2$ . The two disjoint curves (b) and (c) describe a two-part model. Curve (b), for the high-field region, is identical to the lower-energy part of curve (a), but shifted in amplitude and energy, to correspond to a  $10\mu\text{G}$  field; it will give exactly the same radio spectrum as curve (a). Curve (c), for the low-field region, is identical to the high- $\gamma$  part of curve (a), with a small offset for clarity, and produces the same  $\gamma$ -ray emission. If this part of the source has a weak magnetic field,  $B \ll B_{CMB}$ , there will be no detectable radio emission from electrons in curve (c). Right: Example of a sequence of peaked electron spectra, created by Alfvénic ISR, in a range of B fields, as discussed in Section 6.2. Each individual spectrum here is  $n(\gamma) \propto \gamma^2 e^{-(\gamma/\gamma_c)^{3/2}}$ , an example of the steady state kernel created when Alfvénic acceleration balances radiative losses. The peak energy  $\gamma_c$ , can be found from (14) if  $W(k) \propto k^{-3/2}$ . The solid line shows one spectrum with  $\gamma_c = 10^{5.5}$ . The dotted lines show the same function, repeated for a range of lower  $\gamma_c$  values. The spread in  $\gamma_c$  illustrated here can be caused by a spread  $\sim 125$  in B field. The amplitude of each kernel, chosen arbitrarily here to mimic an integrated power law, is determined physically by the fractional volume of the source at the relevant B field.

### 3.4. From theory: inhomogeneous models

The previous models treat the radio lobes as homogeneous systems, with one magnetic field throughout. Turning to theory, however, we expect the B field to have some spatial structure. Basic physics tells us it is hard to create a uniform, single-valued B field throughout a complex plasma structure such as the Cen A lobes.

If the source is inhomogeneous, radio emission will come dominantly from plasma in high-B regions, while the  $\gamma$ -rays come from any part of the source which contains relativistic electrons at the right energies. This can be illustrated with a two-part spectral model, in which localized, high-B regions (radio-loud) coexist with an extended, low-B ( $\gamma$ -ray-loud) plasma. The electron distributions in the two regions may be totally decoupled; curves (b) and (c) of the left panel of Figure 2 show one example. In this situation, the relation between  $U_{e, sy}$  and  $U_{e, ICS}$  (equation 8) no longer applies, so we must abandon the simple result of a quasi-equipartition field throughout the lobes.

We do not know what supports the magnetic field in the radio lobes of Cen A, but MHD theory motivates several possible models.

*Turbulent dynamo.* The outer lobes probably contain turbulence, possibly driven by internal velocity shear. The turbulence will drive a fluctuation dynamo, supporting a mean field,  $B_{turb}^2 \lesssim 4\pi\rho v_t^2$ . (Note the field is dynamically weak if the turbulence is subsonic:  $B_{turb}^2 \propto \mathcal{M}_t^2 p$  where  $v_t$  and  $\mathcal{M}_t$  are the velocity and the Mach number of the turbulence, and  $p$  is the total pressure). While the field is spatially intermittent (obeying a log-normal distribution), simulations suggest that most of the volume is filled with  $B \sim B_{turb}$ , and only a small fraction of volume contains significantly larger fields, especially in the case of subsonic turbulence (*e.g.*, Schekochihin *et al* 2004, Haugen *et al* 2004).

**Table 3.** The range of B field models suggested for the outer lobes of Cen A.

Method	B ( $\mu\text{G}$ )	Comments, where discussed
Minimum radio-loud field <sup>a</sup>	$\gtrsim 0.06\xi^{2/3}$	Plasma pressure balancing IGM pressure (§3.2)
Field at minimum pressure <sup>a</sup>	$\sim 0.6\xi^{2/7}$	Minimum pressure in radio-loud plasma (§3.2)
Homogeneous models <sup>a</sup>	$\sim 1$	Tuned to fit radio and $\gamma$ -ray emission; assumed uniform throughout lobe (§3.3)
Turbulent dynamo <sup>b</sup>	$\sim (2-3)\mathcal{M}_t$	Magnetic field supported by turbulence; spatial fluctuations small if $\mathcal{M}_t \lesssim 1$ (§3.4)
Dynamic balance field	$\sim 3$	Magnetic field balancing IGM pressure; highest field that can be confined by IGM (§3.4)
Shock-enhanced fields <sup>c</sup>	$\sim 10$	Weak shocks throughout source; High B localized to shock regions (§3.4)
Self-organized fields <sup>c</sup>	$\sim 1-10$	Force-free fields throughout source; Large-scale gradients in B (§3.4)

<sup>a</sup> Assumes  $\nu_1 = 10$  MHz ( $\gamma_1 \simeq 4000B_{\mu\text{G}}^{-1/2}$ ) for low-energy cutoff to electron spectrum. The scaling factor  $\xi = (1+k)/\phi$  (see §3.2).

<sup>b</sup>  $\mathcal{M}_t$  is Mach number of turbulence, defined in terms of the adiabatic sound speed; numerical range for  $\Gamma \in (4/3, 5/3)$  and  $p = 3.2 \times 10^{-13}$  dyn cm<sup>-2</sup>.

<sup>c</sup> Magnetic field value is an estimate only, to illustrate an overpressured B field.

*Dynamic balance field.* The largest field that can be in pressure balance with ambient IGM is  $B_{dyn} \simeq (8\pi p_{IGM})^{1/2} \simeq 2.8(n_{-4}T_{\text{keV}})^{1/2}\mu\text{G}$  (using  $p_{IGM}$  from Section 2.3). While the lobes are unlikely to contain a uniform field at this level,  $B_{dyn}$  is a useful fiducial value. Stronger fields must be either transient or self-confined.

*Shocks in transonic turbulence.* Transonic turbulence generates a complex network of shocks, in which high-field fluctuations can become significant (*e.g.*, Molina *et al* 2012). It is tempting to speculate that the radio-bright filaments (apparent in Figure 1) are shocks in transonic turbulence (*e.g.*, Tregillis *et al* 2001). If these are weak shocks (Mach number of a few), simple compression will boost the pre-shock field by a factor  $\gtrsim 2$ . In addition, there is substantial evidence that instabilities set up by streaming cosmic rays enhance the pre-shock magnetic field more strongly than just the modest compression boost (*e.g.*, Riquelme and Spitkovsky 2010; Schure *et al* 2012). For numerical examples I will use  $\sim 10\mu\text{G}$  (roughly ten times higher pressure than lobe plasma not close to any shock).

*Self-organized magnetic structures.* Several authors have suggested that self-organized, nearly force-free fields exist within radio lobes and cavities (*e.g.*, Lynden-Bell 1996; Gourgoulas *et al* 2012). These structures are the end point of magnetic (or Taylor) relaxation, which develops spontaneously if magnetic energy and helicity are injected into the system (*e.g.*, Tang 2008, Benford and Protheroe 2008). In their simplest versions (*e.g.*, Lynden-Bell 1996, Li *et al* 2001), these structures are characterized by magnetically dominated cores within denser, lower-B outer regions. This model connects well to the frequency-dependent width of the north lobe (Section 2.1), which could be caused by a weaker B field towards the outer edges of the source. For numerical examples I will also use  $\sim 10\mu\text{G}$  for the high-field regions in this model.

#### 4. Young models do not work

Some authors have suggested the radio lobes are no older than the radiative lifetimes of their relativistic electrons. In this section I show this cannot be the case.

##### 4.1. Radiative lifetimes of relativistic electrons

Determining radiative lifetimes should be a straightforward application of basic physics. However, we do not know the magnetic field in which a relativistic electron currently sits, let alone that which has felt over its radiative life. I therefore evaluate the maximum possible radiative life, which applies if the particle has spent most of its life in a weak magnetic field,  $B \ll B_{\text{CMB}}$ . Details are given in Appendix A, where the key results are (A.3) and (A.5).

The short lifetime of the  $\gamma$ -ray loud electrons is the most stringent condition on the physics of the outer lobes. Equation (A.3) shows that these electrons (with  $\gamma \sim 3.4 \times 10^5 - 2.8 \times 10^6$ ) live *no longer than* 6.8 Myr for the lower energies, or 0.80 Myr for the higher energies. These upper limits on the lifetime hold if  $B \ll 3.2\mu\text{G}$  (the CMB equivalent field); higher fields will reduce the radiative lifetimes significantly. For example, if  $B \sim B_{\text{dyn}} \sim 2.8\mu\text{G}$ , the lifetime range reduces to 0.47–3.8 Myr; overpressure fields (*e.g.*, Table 3) result in sub-Myr lifetimes for all  $\gamma$ -ray loud energies. Thus, if Cen A is older than  $\sim 1$  Myr, the  $\gamma$ -ray-loud electrons must be undergoing ISR.

The lifetimes of the radio-loud electrons are also relatively short. Because high frequency observations (H09) suggest a spectral turnover around  $\sim 5$  GHz, the maximum lifetime of electrons radiating at that frequency is of interest. From (A.5), the longest possible synchrotron lifetime is  $t_{\text{sy}}^{\text{max}}(5\text{GHz}) \simeq 25B_{\text{now},\mu\text{G}}^{1/2}$  Myr, where  $B_{\text{now}}$  is the field in which the electrons currently sit. The largest plausible value of  $B_{\text{now}}$  might be  $\sim 10\mu\text{G}$  in the radio-loud regions (as in Section 3.4 and Table 3). Even this optimistic estimate would push  $t_{\text{sy}}^{\text{max}}(5\text{GHz})$  only to  $\sim 80$  Myr. If Cen A is older than this, the radio-loud electrons in the outer lobes must also be undergoing ISR.

##### 4.2. The outer lobes can't be as young as they look

It is easy to show that Cen A must be older than the radiative lifetime of its  $\gamma$ -ray-loud electrons. For instance, if Cen A is 1 Myr old, the ends of the outer lobes must have propagated from the AGN at  $\simeq 0.99\mu^{-1}c$ . Even if the lobes lie close to the sky plane, this violates observations: there is no sign of relativistic beaming or sidedness on these large scales. In addition (referring to models I will present in Section 5.3),

near-light-speed propagation of the outer ends would require a relativistic internal flow speed (which also violates observations), and a very low ambient density, (which seems unlikely given Cen A’s central position within its group of galaxies (as in Section 2.3).

Alternatively, various authors have argued that Cen A is no older than the synchrotron age for radio-loud electrons in the outer lobes. H09 estimated  $t_{sy} \sim 30$  Myr for electrons radiating at 5 GHz; they and several authors since have taken this as the true age of the source. Y12 made a similar argument, but chose  $t_{sy} \sim 80$  Myr for electrons radiating at 1 GHz. These ages still violate observations. I will show (in Section 5.3) that growing the radio source so quickly requires highly supersonic flows within the outer lobes. Such flows would be easy to detect, especially their terminal shocks which would be seen as hot spots.

#### 4.3. Ages based on spectral steepening

If the dynamic age of a radio galaxy is not known, the radio and/or  $\gamma$ -ray spectrum of the source is often used to derive a “spectral age” (*e.g.*, H09 or Y12 for Cen A). These calculations make the critical assumption that the relativistic electrons seen in radio or  $\gamma$ -rays are energized only at their initial insertion into the system, after which they undergo only radiative losses. In that situation, the energy at which the electron spectrum steepens is directly related to the elapsed time since the process started, through (A.2) and (A.4). However, this calculation is only a good estimate of the age of the source if we know that no other physics has affected the electrons. Because several possible ISR mechanisms can alter the electron distribution (referring to models I will discuss in Section 6), I argue that spectral ages are not robust unless backed up by independent evidence, for instance from dynamic models of the source’s evolution.

It is worth noting that some spectral-aging models include a variant on the required ISR. These models (*e.g.*, H09, Y12) assume that new electrons are continually “injected” into the radio lobes as the pre-existing electrons cool. The injection mechanism is not specified, but is typically thought of as new particles supplied from the AGN. In Cen A, those electrons would have to travel at nearly lightspeed in order to offset the rapid losses of the existing  $\gamma$ -ray-loud population in the outer lobes. Such fast streaming is difficult given the finite plasma density and disordered magnetic field likely to exist in the lobes. One might argue instead that the new electrons are injected locally, pulled from a thermal population by shock or turbulent acceleration (as in Section 6). This is possible, but if such processes exist, they would also provide ISR for the existing relativistic electrons, thus modifying the energy spectrum of those electrons and undermining any simple relation between spectral break energy and source age.

### 5. Older models which may work

In the previous section I argued that the radiative lifetimes of the relativistic electrons in Cen A are shorter than any plausible dynamical age of the radio lobes. In this section I justify this assertion with three simple models for growth of the outer lobes: a buoyant plume, a magnetic tower, and a flow-driven model. Two timescales set the stage for what follows.

*The sound-crossing time in the IGM.* Using the adiabatic sound speed, ( $c_s^2 = \Gamma kT/\bar{m}$  with adiabatic index  $\Gamma = 5/3$  and mean particle mass  $\bar{m} = 0.6m_p$ ) and

recalling the length of the source is  $D \sim 300/\mu$  kpc, the sound crossing time over this distance in the IGM is

$$\tau_{sound} = \frac{D}{c_{s,IGM}} \sim \frac{570}{\mu T_{keV}^{1/2}} \text{ Myr} \quad (9)$$

I will show in this section that  $v_{end} \lesssim c_{s,IGM}$  for the two slower models (buoyant plumes and magnetic towers), so that Cen A must be at least as old as  $\tau_{sound}$ . In a momentum-driven flow, I will show that the age of the source can be pushed down to perhaps half of  $\tau_{sound}$ , but no younger.

*The time needed to excavate the outer lobes.* The enthalpy content of an outer lobe is  $\Gamma pV/(\Gamma - 1) \sim 1.8 \times 10^{59}/\mu$  erg if the lobe plasma is internally subrelativistic ( $\Gamma = 5/3$ ), or  $\sim 2.9 \times 10^{59}/\mu$  erg if the plasma is internally relativistic ( $\Gamma = 4/3$ ). Scaling the time-averaged power from the AGN to its current strength ( $P_{AGN} = 10^{43} P_{43}$  erg/s to each side of radio source; Section 2.2), we can estimate the time needed to excavate the outer lobes:

$$\tau_{exc} = \frac{\Gamma}{\Gamma - 1} \frac{pV}{P_{AGN}} \sim \frac{570-910}{\mu P_{43}} \text{ Myr} \quad (10)$$

This expression assumes the plasma within the lobe is dominated by thermal energy; the numerical range is for  $\Gamma \in (4/3, 5/3)$ . If the lobe contains significant transonic flows or dynamically strong magnetic fields the excavation time will be longer than these values.

**Table 4.** Summary of dynamic models for outer lobes; see text for details.  $\mu$  is the cosine of the angle between the radio lobes and the sky plane.

	Buoyant plume	Magnetic tower	Flow-driven lobe
Advance speed	$v_{end} < c_{s,IGM}$	$v_{end} \sim c_{s,IGM}$	$v_{end} > c_{s,IGM}$
Age	$\gtrsim 570/\mu$ Myr	$\sim 570/\mu$ Myr	$\sim (300-600)/\mu$ Myr
Necessary conditions	internally subsonic	high-B plasma core	internally transonic
Magnetic structure	turbulent dynamo, small-scale fluctuations	large-scale order, large-scale gradients	high-B (shocks), low-B (intershock)
ISR mechanism	Alfven turbulence	reconnection + Alfven turbulence	shock acceleration + Alfven turbulence

The three models to be described in this section are closely connected to the different magnetic field models (described in Section 3), and also to the competing ISR mechanisms (to be described in §6). To help the reader keep it all straight, in Table 4 I summarize the three models including their probable connections to B field structure and ISR mechanisms.

### 5.1. Slower growth: buoyant plumes

The plasma at the outer end of a mostly-hydrodynamic radio lobe feels two forces, buoyancy (assuming the lobe is less dense than the ambient IGM), and ram pressure (from fluid coming in behind it). The slowest growth happens when buoyancy drives the lobe. We know, of course, that the outer lobes of Cen A do not resemble the

turbulent, entraining plumes which some authors (*e.g.*, Bicknell 1984, DeYoung 1986) have suggested as models for tailed radio galaxies. The outer lobes do not show the gradual broadening, going away from the source, which is characteristic of such plumes. Nor is there any sign of the lateral spreading expected if the end of a plume has reached the neutral buoyancy level in the surrounding IGM. However, the growth of the outer lobes may still be dominated by buoyancy if the buoyant force exceeds ram pressure force at the end of the lobe.

There is not much work in the fluid literature describing the advance speed of the end of a driven buoyant plume, but we can estimate an upper limit. We know that the speed at which a small buoyant bubble rises through an atmosphere is determined by the balance of buoyant and drag forces. If the ambient medium is hydrostatic, in the gravity of the galaxy group, it is easy to show that this buoyant rise speed is no larger than the sound speed in the external medium, and very likely much less. We can speculate that a similar limit applies to the buoyancy-dominated end of a continuous plume, so that the end advances into the IGM at  $v_{\text{end}} \lesssim c_{s, \text{IGM}}$ . Thus, the age of a buoyancy-driven radio lobe will be at least as long as  $\tau_{\text{sound}}$ , and probably longer.

The internal state of a buoyancy-driven radio lobe is probably close to the homogeneous models of Section 3.3. Nothing in the model calls for large-scale spatial gradients. Some level of MHD turbulence is likely, and indeed is necessary for ISR (as will be shown in Section 6); but if the turbulence is subsonic, it does not induce significant inhomogeneities (Section 3.4)

### 5.2. Intermediate growth: magnetic towers

An alternative model obtains when the AGN power creating the radio lobes is dominated by the magnetic field. Although some plasma flow can be included in a classic magnetic tower, the energy is mostly carried by Poynting flux (Lynden-Bell 1996, Li *et al* 2001). Numerical models of magnetic towers propagating into an ambient IGM (*e.g.*, Nakamura *et al* 2006) show a magnetically dominated interior, with the field close to a force-free configuration. As the tower grows, it comes into lateral pressure balance with the IGM; hoop stresses concentrate the field toward the axis and maintain lateral collimation, while allowing vertical growth as the front end advances into the IGM (*e.g.*, Uzdensky and MacFadyen 2006). Both analytic models and simulations show the end advances at  $v_{\text{end}} \sim c_{s, \text{IGM}}$  into the IGM (Lynden-Bell 1996, Nakamura *et al* 2006). The growth rate of other self-organized models, such as those suggested by Tang (2008) or Benford and Protheroe (2008) has not been worked out, but we might guess that such structures develop similarly to magnetic towers.

Because the internal state of a magnetically self-organized radio lobe includes large-scale gradients in both the B field strength and the plasma density, these models are among the inhomogeneous-field models discussed in Section 3.4.

### 5.3. Faster growth: flow-driven lobes

If organized plasma flow from the AGN continues to the end of the outer lobes, ram pressure can dominate the growth of the lobe and grow the source faster than buoyancy or magnetic pressure. A simple model can illustrate this idea, which I summarize here; details are given in Appendix B.

Assume a channel flowing within each radio lobe carries all of the energy and momentum to drive the lobe. At the outer end of the lobe – which advances less



rapidly than the speed of the plasma within the channel – that plasma must slow down and move aside. The channel will therefore be surrounded with a “cocoon” which acts as a reservoir for mass and energy from the channel. This cocoon is the observed radio lobe. This model derives, of course, from standard models of FR II radio sources, but must be modified to agree with the lack of strong outer hot spots in FRI sources. The model has two important parts, as follows.

(1) The advance speed of the end,  $v_{end}$ , is governed by momentum conservation, where the outer end of the channel impacts the IGM. The momentum flux carried by the channel will be spread over an area ( $A_{end}$ ) at least as large as the area of the channel ( $A_c$ ), and possibly larger. If the channel impacts the end of the lobe with density  $\rho_c$  and speed  $v_c$ ,  $v_{end}$  is governed by  $\rho_{IGM}v_{end}^2 \lesssim \rho_c v_c^2$  (B.2, B.4). If the lobe and IGM are also in pressure balance, and the end propagates supersonically into the IGM, the channel flow must be *internally* transonic:  $\Gamma_c \mathcal{M}_c^2 \gtrsim \Gamma_{IGM} \mathcal{M}_{end}^2$  (B.3, B.4). The lower limits on  $v_c$  and  $\mathcal{M}_c$  obtain when  $A_{end} \rightarrow A_c$ ; if the momentum flux is spread over a larger impact area, the advance speed  $v_{end}$  is correspondingly lower.

(2) The flow power in the channel,  $P_c$ , can be found directly from energy conservation, if we account for growth of the lobe volume and work done on the IGM. This calculation depends on the aspect ratio  $a/D$  of the lobe: if the lobe grows self-similarly, with  $a/D$  remaining constant, more power is required to grow the lobe at a given  $v_{end}$  than if the lobe radius  $a$  remains constant. I parameterize this uncertainty with a factor  $1 \lesssim f_V \lesssim 3$ , describing the range from constant-radius growth to self-similar growth. The general result for  $P_c$ , (B.7), contains two terms: one describing the growth of the full lobe, and an additional factor describing the extra power needed to maintain the channel flow. As with the advance speed, the result  $P_c$  depends on the working surface area,  $A_{end}$ . The minimum  $P_c$  needed to grow the source, (B.9), occurs when  $A_{end} \rightarrow A_c$ ; for larger  $A_{end}$  values, higher power is needed.

**Table 5.** Flow-driven models for outer lobes. Models assume lobe length  $300/\mu$  kpc, lobe radius  $a = 90$  kpc, and pressure  $p = 3.2 \times 10^{-13} \text{ dyn cm}^{-2}$ .  $f_V \in (1, 3)$  describes the geometry of the expanding lobe.  $\mu$  is the cosine of the angle between the radio lobe and the sky plane.  $r_c/a$  is the ratio of channel radius to lobe radius. The minimum value of  $P_c$ , from (B.9), is reached when momentum flux is exerted only over the area of the channel; a larger working area requires a larger  $P_c$ .

Age (Myr)	$v_{end}$ (km s $^{-1}$ )	$\mathcal{M}_{end}^a$	$\mathcal{M}_c^a$	Power carried in channel <sup>b</sup> (erg s $^{-1}$ )	comments
$30/\mu$	9800	25.	$\gtrsim 25$ .	$P_c \gtrsim 1.9f_V \times 10^{44} [1 + 600r_c^2/a^2]$	unlikely
$100/\mu$	2900	7.5	$\gtrsim 7.5$	$P_c \gtrsim 5.6f_V \times 10^{43} [1 + 56r_c^2/a^2]$	unlikely
$300/\mu$	980	2.5	$\gtrsim 2.5$	$P_c \gtrsim 1.9f_V \times 10^{43} [1 + 6.3r_c^2/a^2]$	challenging
$600/\mu$	480	1.2	$\gtrsim 1.2$	$P_c \gtrsim 9.3f_V \times 10^{42} [1 + 1.4r_c^2/a^2]$	possible

<sup>a</sup> The internal Mach number of the channel is  $\mathcal{M}_c = v_c/c_{s,c}$ ; the Mach number of the end relative to the IGM is  $\mathcal{M}_{end} = v_{end}/c_{s,IGM}$ .

<sup>b</sup> Values for  $P_c$  assume  $\Gamma_c = \Gamma_{IGM} = 5/3$ ; if  $\Gamma_c = 4/3$ , the leading term in  $P_c$  would increase by 1.6; the second term inside brackets would decrease by 0.6.

To apply this analysis, we can choose a source age,  $\tau$ , and find the necessary end speed ( $v_{end} = D/\tau$ ). Because we are searching for models in which the source

is younger than  $\tau_{\text{sound}}$ , we require supersonic propagation of the end into the IGM:  $v_{\text{end}} \gtrsim c_{s, \text{IGM}}$ . I keep  $r_c/a$  as a free parameter, but note that spectral tomography of some FRI sources (Katz-Stone and Rudnick 1996, Katz-Stone *et al* 1999) suggests that  $r_c$  is not too small a fraction of the source radius (perhaps  $r_c/a \sim 1/3 - 1/2$ ). Putting these choices into (B.9), along with values of the lobe radius  $a$  and ambient pressure  $p_{\text{IGM}}$ , gives the power needed to grow the source at rate  $v_{\text{end}}$ . Table 5 presents a range of choices for  $v_{\text{end}}$ , with the associated source ages, Mach numbers and required core powers. By keeping two criteria in mind, we immediately see that the younger models cannot work for Cen A. (1) Cen A does not have bright outer hot spots. This alone rules out the younger models, because Mach numbers  $\mathcal{M}_c \gtrsim 2 - 3$  will create a strong shock at the outer end; such a shock would be highly visible as a radio-loud hot spot. (2) Younger models require a much higher core power in the past, averaged over the age of the source, than the power now being put out by the AGN ( $\sim 10^{43} \text{erg/s}$ , Section 2.2). This is especially true if  $r_c \lesssim a$ , but holds even if  $r_c \ll a$  (which would suggest a very small, very bright outer hot spot). Of course it may be that the AGN in Cen A is currently running at much lower power than it has over most of its active life – but such models are unattractive.

The internal state of a flow-driven lobe will very likely be turbulent, driven for instance by internal shear flows (also see Tregillis *et al* 2001). Because the internal flows in the most plausible models are transonic with  $\mathcal{M}_c \sim 1 - 2$ , the turbulence they drive will include weak shocks throughout the radio lobes. Thus, these models are included in the inhomogeneous models discussed in Section 3.4.

#### 5.4. Compare dynamic models to the data

The simple models presented so far have been general, and might apply to any FRI-type of radio galaxy. How well do they do when confronted specifically with the data? Key observational results on Cen A are as follows.

- *Morphology.* Both lobes have a generally uniform brightness distribution. There is no sign of hot spots or any surface brightness enhancement towards the outer ends. The outer lobes are not limb brightened, but rather center filled (as shown by slices through the image in Figure 1). Their brightness distribution is not totally smooth, however. Some large-scale features ( $\sim 30 - 60 \text{ kpc}$ ) exist in each lobe, including the Northern Loop (Junkes *et al* 1993) and a low surface brightness “hole” at the outer end of the north lobe; a similar region on the southeast edge of the south lobe; and the vertex/vortex structure in the southern lobe (Feain *et al* 2011).
- *Limb darkening.* As mentioned in Section 2.1, the size of each lobe depends on the observing frequency. The north lobe is significantly broader in  $\gamma$ -rays than in radio (Y12). In radio, the full length of both lobes is detected only below  $\sim 10 \text{ GHz}$  (H09); the full radio width of the north lobe is seen only below  $\sim 1 \text{ GHz}$  (apparent by comparing low-frequency radio images, from McKinley *et al* 2013 and Stefan *et al* 2013, to the  $5 \text{ GHz}$  image from Junkes *et al* 1993). Without the  $\gamma$ -ray data, this would normally be interpreted as spectral aging (plasma in the extremities of the lobes is older and the electron spectrum has steepened there; *cf.* Section 4.3). However, because we know that ISR is needed for the both the  $\gamma$ -ray-loud and radio-loud electrons, passive spectral aging is not the answer. Large-scale gradients in the B field and/or the ISR mechanism must exist in the radio lobes.

- *Polarization.* Both lobes show strong, ordered, large-scale polarization. Parts of both lobes are polarized up to 30-50% on scales  $\sim 60-70$  kpc (Junkes *et al* 1993). As with other radio galaxies, the polarization vectors in Cen A tend to correlate with local geometry. The component of the B field in the sky plane tends to lie along bright ridges or filaments or along the outer edges of the radio lobes. These data strongly constrain any model of small-scale, isotropic magnetic turbulence within lobes, because any more than a few random magnetic “cells” along the line of sight would significantly depolarize the signal (*e.g.*, Burn 1966).
- *Filaments.* The outer lobes are filled with striking filamentary structures apparent in Figure 1. The filaments are not sparse; they have a covering factor close to unity. The lack of limb brightening rules out edge effects (*e.g.*, surface instabilities) as the cause of the filaments; they must be internal to the lobes. Measurement of a few bright filaments reveals a typical width of a few kpc and a typical emissivity enhancement of a factor of  $\sim 10$  (relative to the mean lobe emissivity, assuming cylindrical filaments).

How do the three dynamic models fare against these data?

- *Buoyant models.* Because this model is to first-order internally homogeneous, it is consistent with uniform, center-filled lobes. However, just because of that homogeneity, the model is severely challenged by the large-scale polarized structures, frequency-dependent limb darkening and high-contrast radio filaments. Additional physics will be needed to explain these phenomena – for instance the effects of a subsonic flow entering the lobe from the AGN.
- *Magnetic towers.* Because this model invokes system-scale gradients in the B field, it is easily compatible with large-scale polarized structures as well as the observed limb darkening. Simple axisymmetric versions of the model (*e.g.*, Nakamura *et al* 2006) fail because they predict a radio-faint central cavity that is not seen. Spatially more complex models may avoid this problem, and may also provide a possible explanation of the filaments (*e.g.*, Tang 2008). However, these models have not yet been developed to where they can be robustly tested against the data.
- *Flow-driven models.* Because this model is intrinsically two-part (a channel flow within a surrounding cocoon), it agrees well with center-filled emission and has the potential to explain *lateral* limb darkening as well (if physical conditions in the cocoon are sufficiently different from those in the channel). Internal shocks driven by transonic flow provide an attractive model of the filaments, and may exist on large-enough scales to account for the large-scale polarized features. The model is seriously challenged, however, by the lack of any sign of channel deceleration or spreading towards the outer ends of the lobes.

This comparison shows that the internally homogeneous, buoyant model does the poorest job of matching the data. The magnetic tower and flow-driven models do better, but objections can be made to simple versions of each one. Furthermore, any successful dynamic model of Cen A must incorporate one or more ISR mechanisms; that is the topic of the next section. In Table 6 I summarize how well, or badly, each of the dynamic models compare to the data.

**Table 6.** Critique of models suggested for Cen A. Buoyant model assumes Alfvénic ISR; magnetic tower assumes reconnection and Alfvénic ISR; flow-driven model assumes shock and Alfvénic ISR.

	Buoyant plume	Magnetic tower	Flow-driven lobe
Center-filled lobes	easy	possible <sup>a</sup>	easy
Large-scale polarization	hard	easy	possible <sup>a</sup>
Lateral limb darkening	hard	easy	needs work <sup>b</sup>
Outer end limb darkening	hard	needs work <sup>b</sup>	hard
Radio-bright filaments	challenging	needs work <sup>b</sup>	easy
Radio- $\gamma$ -ray power ratio	challenging	easy	easy
Steep $\gamma$ -ray spectrum	needs work <sup>b</sup>	needs work <sup>b</sup>	needs work <sup>b</sup>
Power-law radio spectrum	challenging	probable <sup>c</sup>	easy

<sup>a</sup> “Possible” means the model satisfies the criterion if conditions are right within the source (large-scale shocks in flow-driven model; high-order modes excited in magnetic tower models.)

<sup>b</sup> “Needs work” means that relevant models not yet sufficiently developed to meet the data (nature of the cocoon for flow-driven models; distribution of radio emissivity in magnetic tower models; high-energy end of particle spectrum in ISR models).

<sup>c</sup> “Probable” means model works if current theories of reconnection ISR are valid.

## 6. In situ reacceleration in the outer lobes

In the previous section I showed that the outer lobes of Cen A are much older than radiative lifetime of the relativistic electrons which make the lobes shine in radio and  $\gamma$ -rays. This proves that ISR is required throughout the outer lobes. In this section I discuss how that might happen. I begin by demonstrating that diffusion is likely to be slow within the radio lobes, so that local (in situ) reacceleration is needed. I then discuss three competing ISR models – Alfvén wave turbulence, shocks and reconnection – in the specific context of dynamic models I have introduced for Cen A. I argue that Alfvénic ISR is probably the most likely mechanism in all three models, but that it is not yet well enough understood to confront the data fully. I also argue that shock and reconnection ISR are very attractive alternatives *if* the necessary conditions exist within the outer lobes.

As a prelude to this discussion, note that all three ISR models are sensitive to particle scattering on microphysical scales (possibly as small as the gyroradius,  $r_L = \gamma mc^2 / eB$ ). ISR models generally assume this scattering exists, with some mean free path  $\lambda_{mfp}$ . Unfortunately,  $\lambda_{mfp}$  is not well understood. Some authors assume the optimistic Bohm limit, in which  $\lambda_{mfp} \sim r_L$ , but detailed modelling suggests the Bohm limit is not often reached, and scattering on a spectrum of MHD waves may be better described by quasi-linear (QL) theory (*e.g.*, Casse *et al* 2003; Dosch *et al* 2011).

In the usual QL approach, Alfvén wave turbulence is assumed to exist throughout the source. Let it have a spectrum  $W(k)$ , normalized so that the turbulent energy density is  $u_{turb} = \int W(k) dk$ . Relativistic particles at energy  $\gamma$  interact most strongly with waves at their resonant wavenumber,  $k_{res}(\gamma) \simeq eB / \gamma mc^2$  (equivalently, with

resonant wavelength  $\lambda_{res} \simeq r_L$ ). If  $W(k)$  decreases with  $k$  above some driving scale  $k_{min} = 2\pi/\lambda_{max}$ , we can write  $u_{turb} \sim k_{min}W(k_{min})$  for the total turbulent energy, and  $u_{res}(\gamma) \sim k_{res}(\gamma)W[k_{res}(\gamma)]$  for the energy in waves at or above the resonant wavenumber. Because the ratio  $u_{res}(\gamma)/u_{turb}$  is critical in what follows, we must develop numerical estimates, as follows.

To estimate  $\lambda_{max}$  in Cen A, we recall fluid flows, where  $\lambda_{max}$  is commonly taken as some large fraction of the channel width. In Cen A, we might also use the loops and filaments in the radio image to estimate  $\lambda_{max}$ ; inspection of the image in Figure 1 shows their scale is also some large fraction of the lobe width. Based on these arguments, I will scale  $\lambda_{max}$  to 30 kpc. For comparison, the resonant wavelength of  $\gamma \sim (0.34 - 2.8) \times 10^6$  electrons seen in  $\gamma$ -rays is  $r_L(\gamma) \simeq (0.7 - 5.6) \times 10^{15}/B_{\mu G}$  cm, so that  $k_{res}(\gamma) \gg k_{max}$ .

We also need the ratio  $u_{res}(\gamma)/u_{turb}$ , which measures the fraction of turbulent energy in resonant waves. It is traditional in the literature to represent the wave spectrum as a power law,  $W(k) \propto k^{-r}$ , with  $r \in (1, 2)$  typically. If this assumption is correct,  $u_{res}(\gamma)/u_{turb} = (k_{res}(\gamma)/k_{min})^{-(r-1)} \ll 1$ ; only a very small fraction of the total turbulent energy is available to interact resonantly with the high- $\gamma$  particles we can observe. This  $k^{-r}$  spectrum is commonly invoked in turbulence studies (*e.g.*, Zhou *et al* 2004 and references therein) and found in numerical simulations which assume a low- $k$  driver (*e.g.*, Schekochihin *et al* 2004). However, these results may not be the last word. Bicknell & Melrose (1982) speculated that strong coupling between Alfvén and magnetosonic waves will subject Alfvén waves to the strong damping that magnetosonic waves suffer and terminate the cascade at wavenumbers well below  $k_{res}(\gamma)$ . In addition, modern work such as Brunetti *et al* (2004) considers more general possibilities for wave generation, and thus more general wave spectra than the simple  $k^{-r}$  power law. In this section I will use this simple power law for numerical examples, but the reader should be aware that the real situation may be more complicated.

### 6.1. Need for distributed reacceleration

It is easy to show that ISR sites must be distributed throughout the outer lobes. If the B field within the lobes is turbulent, propagation away from ISR sites will be by diffusion, as the particles scatter on MHD turbulence. § If tangled field lines extend throughout the lobes, particles will diffuse along the field lines at a rate described by a coefficient  $\kappa_{\parallel} \simeq c\lambda_{mfp}/3$ . As discussed above, some authors assume Bohm diffusion applies, with  $\kappa_{\parallel} = \kappa_B \simeq cr_L/3$ . This is the slowest diffusion likely for this geometry. Alternatively, other authors (*e.g.*, Casse *et al* 2003) find the true behavior is closer to the coefficient predicted by QL theory,

$$\kappa_{\parallel} \simeq \frac{24}{\pi\eta} \kappa_B \frac{u_{turb}}{u_{res}(\gamma)} \quad (11)$$

where  $\eta = u_{turb}/u_B$  is the ratio of turbulent to total magnetic energy.

For  $k_{res} \gg k_{min}$ , and a wave spectrum  $W(k)$  which decreases with  $k$ , clearly  $\kappa_{\parallel} \gg \kappa_B$ . However, we are lucky here: despite the large uncertainty in the correct value of  $\kappa_{\parallel}$ , we can show that the distance a relativistic electron travels from its origin is small. Recall that any ISR mechanism must be able to offset the most rapid radiative losses, with lifetimes only a few Myr for the  $\gamma \gtrsim 10^6$  electrons which radiate

§ If the B field is ordered, as in magnetic tower models, the particles can stream along field lines at the Alfvén speed, but much slower cross-field propagation is diffusive.

at the high end of the  $\gamma$ -ray band. For example, picking  $B = 1\mu\text{G}$  and  $\gamma = 10^6$  and assuming QL scattering, the diffusion distance in 1 Myr is only  $\sim (4\kappa_{\parallel}t_{\text{rad}})^{1/2} \sim 16$  kpc for  $\gamma$ -ray loud electrons. If Bohm diffusion rules, the diffusion distance is much smaller, less than a kpc. (Different choices for  $B, \lambda_{\text{max}}$  and the turbulent exponent  $r$  do not affect this qualitative conclusion.) Thus – because the diffusion distance is so small – we see that ISR sites must exist throughout the outer lobes.

### 6.2. Alfvén turbulent acceleration

This ISR mechanism is commonly invoked for diffuse nonthermal plasmas, including radio galaxies in general (*e.g.*, Lacombe 1977, Eilek 1979), and Cen A in particular (H09, O’Sullivan *et al* 2009, Wykes *et al* 2013). Relativistic particles scatter on resonant waves and slowly diffuse in momentum space, in a second-order ISR process.

*Acceleration rates.* Two conditions must be met in order for Alfvénic acceleration to be a useful model for Cen A. The first condition is speed: the acceleration time,  $t_{\text{acc}}$ , must be no longer than the radiative loss time,  $t_{\text{rad}}$  (from A.1). To determine  $t_{\text{acc}}$ , we can follow standard QL theory (*e.g.*, Lacombe 1977) to determine the momentum diffusion coefficient,<sup>¶</sup>

$$D_p \simeq \frac{\pi^2 e^2 v_A^2}{c^3} W[k_{\text{res}}(p)] \quad (12)$$

This expression is, of course, closely related to the QL diffusion coefficient (11), because both processes depend on resonant particle scattering by Alfvén waves. From (12) we can estimate the acceleration time,

$$t_{\text{acc}}(\gamma) \simeq \frac{p^2}{D_p} \simeq \frac{8}{\pi} \frac{\gamma mc}{eB} \frac{1}{\eta \beta_A^2} \left[ \frac{u_{\text{turb}}}{u_{\text{res}}(\gamma)} \right] \quad (13)$$

This form shows that acceleration is faster for higher  $\eta = u_{\text{turb}}/u_B$ , higher  $\beta_A = v_A/c$ , and higher fractional resonant wave energy,  $u_{\text{res}}/u_{\text{turb}}$ . To illustrate, we can assume  $\eta = 1$ , and again use simple power law wave spectrum,  $W(k) \propto k^{-r}$ , with  $r = 5/3$ ,  $\lambda_{\text{max}} = 30$  kpc. Using these in (13), with  $\gamma = 10^6$ , we find  $t_{\text{acc}}(\gamma) \lesssim 1$  Myr if  $v_A \gtrsim 4100$  km s<sup>−1</sup>. This is a key result: because Alfvénic acceleration is slow,  $v_A$  must be high if Alfvénic turbulence is to keep the radio lobes of Cen A shining.

*Problems with the simple model.* Speed isn’t everything, however. A model of ISR must also produce an electron energy distribution,  $n(\gamma)$ , which corresponds to observed synchrotron and ICS spectra. *This is a major problem for this simple model.* In the context of the homogeneous-field model (Section 3.3, also curve (a) of the left panel of Figure 2),  $n(\gamma)$  must be a power law at lower energies ( $\gamma \lesssim 10^5$  in a  $\mu\text{G}$  field), and steepen strongly into and through the ICS range. However, in a steady state, particle-conserving situation, turbulent Alfvénic acceleration in the presence of

<sup>¶</sup> This example used  $B = 1\mu\text{G}, B_{\text{rad}} = 3\mu\text{G}, \eta = 1, r = 5/3$  for a Kolmogorov spectrum and  $\lambda_{\text{max}} \sim 30$  kpc. The diffusion coefficients are then  $\kappa_B \simeq 2 \times 10^{25} \text{cm}^2 \text{s}^{-1}$  and  $\kappa_{\parallel} \simeq 2.0 \times 10^{31} \text{cm}^2 \text{s}^{-1}$ .

<sup>¶¶</sup> This expression approximates equation 9 of Lacombe (1977), with  $p = \gamma mc$ ; note the exact numerical coefficient of  $D_p$  depends on details of the wave field directionality, which vary author to author.



radiative losses creates an electron energy distribution which is *peaked* at the energy where  $t_{rad}(\gamma) \simeq t_{acc}(\gamma)$ :

$$\gamma_{c,A}^2 \simeq \frac{3\pi^2}{4} \frac{e}{\sigma_T} \frac{B}{B_{net}^2} \eta \beta_A^2 \left[ \frac{u_{res}(\gamma)}{u_{turb}} \right] \quad (14)$$

(Borovsky and Eilek 1986, Stawarz and Petrosian 2008). Electrons on the high-energy side of such a peaked distribution may explain the steep  $\gamma$ -ray spectrum, but cannot explain the broadband, power-law radio spectrum (as in the left panel of Figure 2). Thus the simple model must be extended if Alfvénic ISR is to explain the full spectrum from Cen A.

One extension is to a spatially variable magnetic field, say from large-scale gradients in the radio lobes. A range of B fields will broaden the effective electron energy distribution (as in the right panel of Figure 2). This broad  $n(\gamma)$  will in turn distribute the synchrotron kernel function (which peaks at  $\nu_{sy} = aB\gamma_c^2(B)$ ) in frequency, creating a broader, possibly power-law radio spectrum (Eilek and Arendt 1986). Another extension of the model lets the wave spectrum vary in time and space, deviating from the usual power law. Brunetti *et al* (2004) present a specific example which results in a broad, slowly varying  $n(\gamma)$  distribution. Finally, a third extension invokes localized injection of low-energy electrons throughout the radio lobe, enabling Alfvénic ISR to create a broader electron  $n(\gamma)$  (*e.g.*, Borovsky and Eilek 1986). This injection could be provided by nearby shocks or reconnection sites, both described in the next subsection.

### 6.3. Additional ISR mechanisms

While Alfvénic ISR is the mechanism most commonly invoked for the diffuse radio lobes of Cen A, shock acceleration and reconnection acceleration are two attractive alternatives if conditions within the source enable these mechanisms to work.

*Shock acceleration.* Although not often considered for ISR in diffuse radio galaxy lobes, shock acceleration is commonly invoked to explain galactic cosmic ray acceleration in supernova remnants, and ISR in radio galaxy jets and hot spots. It is well known that particles scattering on self-generated turbulence on either side of a shock are accelerated into a power law energy distribution which agrees well with observed synchrotron spectra (*e.g.*, Drury 1983). Because this first-order process is fast, we can envision a shock as a localized “injection event”, very quickly boosting pre-shock particles to high energies.

We must, however, be aware of a major uncertainty in shock theory, namely the scattering mean free path,  $\lambda_{mfp}$  (usually expressed in terms of the shock diffusion coefficient,  $\kappa_s \sim c\lambda_{mfp}/3$ ). As mentioned in Section 6.1, some authors assume Bohm diffusion (the best case for rapid shock acceleration, *e.g.*, Kang 2011), but others assume QL scattering (*e.g.*, Giacalone 2005). We should also note that  $\kappa_s$ , close to the shock, is not necessarily the same as  $\kappa_{\parallel}$  elsewhere in the diffuse radio lobe; the turbulence is likely to be quite different in the two regions.

Keeping this uncertainty in mind, we can nonetheless check the energy range attainable, and compare it to the apparent steepening around  $\sim 5$  GHz in the radio spectrum of Cen A. The timescale for diffusive shock acceleration is  $t_{acc}(\gamma) \simeq F(s)\kappa_s/v_s^2$ , where  $v_s$  is shock speed and  $F(s) = 3s(s+1)/(s-1)$  depends on the shock compression ratio  $s$  (*e.g.*, Drury 1983). Shock acceleration in the presence

of radiative losses will create a power law electron  $n(\gamma)$ , up to the energy at which  $t_{rad}(\gamma_c) \simeq t_{acc}(\gamma_c)$ :

$$\gamma_{c,s}^2 \simeq \frac{18\pi}{F(s)} \frac{\kappa_B}{\kappa_s} \frac{e}{\sigma_T} \frac{v_s^2}{c^2} \frac{B}{B_{net}^2} \quad (15)$$

To illustrate, let the physical field be  $10\mu\text{G}$ , and choose  $s = 2$  for a weak shock. Scaling  $v_s$  to  $10^3 \text{ km s}^{-1}$ , and  $\kappa_s$  to  $\kappa_B$ , we get  $\gamma_{c,s} \simeq 1.5 \times 10^7 v_{s,3} (\kappa_B/\kappa_s)^{1/2}$ . Comparing to Figure 2, we see that – if Bohm diffusion holds –  $\gamma_{c,s}$  is high, well above  $\gamma_{br} \lesssim 10^5$  needed for the 5-GHz spectral break in the high-B region. We can speculate on two possible ways to reconcile this estimate for  $\gamma_{c,s}$  with the data. Because radiative losses are rapid for these high  $\gamma$ 's, electrons at  $\gamma \sim \gamma_{c,s}$  will lose most of their energy very quickly. Noting that radio observations cannot resolve the small postshock regions, the observed spectral break may mean we are seeing most of the electrons a few Myr after they've been shocked. Alternatively, Bohm diffusion may be too optimistic. If  $\kappa_s \gg \kappa_B$  we could be seeing the intrinsic high- $\gamma$  cutoff of the power law created by shock acceleration.

*Reconnection acceleration* The theory of reconnection ISR is still a work in progress; even the basic physical picture is not yet agreed on. We can explore this mechanism with a simple, two-dimensional reconnection model, as follows. Let two regions of oppositely directed B field be separated by a thin dissipation layer. The plasma on each side of the layer flows in, at some  $v_{in}$ , inducing an electric field  $\mathcal{E} \simeq v_{in}B/c$ . Magnetic energy dissipated in this reconnection layer goes to plasma heating and/or acceleration of suprathermal particles. Particles within this region are subject to two different types of energization – parallel and perpendicular.

One ISR possibility is parallel energization within the reconnection layer. This occurs if the particle moves unimpeded through some (large) distance,  $\lambda_{\parallel}$ , along the inductive potential drop created by the inflow (*e.g.*, Litvinenko 1999, Romanova and Lovelace 1992, Benford and Protheroe 2008). The key requirement here is that  $\lambda_{\parallel}$  be large (compared to microscales such as the electron Larmor radius); this is the opposite limit to strong, Bohm-like scattering. In this situation, the particle gains energy  $\Delta E \simeq e\mathcal{E}\lambda_{\parallel}$ , or

$$\gamma_{\parallel} \simeq \frac{eB}{mc^2} \beta_{in} \lambda_{\parallel} \quad (16)$$

where  $\beta_{in} = v_{in}/c$ . Detailed modelling shows that reconnection events form substantial nonthermal tails, for  $\gamma \lesssim \gamma_{\parallel}$ . These tails are often interpreted as power laws, but this is still an active research area (*e.g.*, Kagan *et al* 2013 and references therein). As a simple example, we can guess  $B \sim 1\mu\text{G}$ , and  $\lambda_{\parallel} \sim 1 \text{ kpc}$ . If we also take  $v_{in} \sim 300 \text{ km s}^{-1}$  (on the order of 10% of  $v_A$  suggested in Section 6.2), we get  $\gamma_{\parallel} \sim 2 \times 10^9$ , easily high enough to keep Cen A shining. However, both  $\lambda_{\parallel}$  and  $v_{in}$  are very sensitive to local conditions; I return to this issue later in this section.

The other ISR possibility is perpendicular energization across the reconnection layer. If the plasma in the region is sufficiently turbulent, particles will scatter back and forth in the converging inflow, gaining energy in a first-order Fermi process (*e.g.*, de Gouveia dal Pino and Lazarian 2005, also Drury 2012). Just as with shock acceleration, the key step here is the strength of the turbulent scattering, measured by  $\lambda_{mfp}$ . The acceleration time given by Drury (2012) can be approximated, for our

simple reconnection-layer picture, as  $t_{acc} \sim 3\lambda_{mfp}/v_{in}$ .<sup>+</sup> The power-law  $n(\gamma)$  created in this process will extend up to an energy at which  $t_{acc}(\gamma_c) \simeq t_{rad}(\gamma_c)$ , or

$$\gamma_{c,rec}^2 \simeq 2\pi \frac{r_L}{\lambda_{mfp}} \frac{e}{\sigma_T} \beta_{in} \frac{B}{B_{net}^2} \quad (17)$$

Illustrating again with a 1μG field,  $B_{net}^2 = 8\pi(u_B + u_{CMB})$ ,  $\beta_{in} \sim 10^{-3}$  and guessing  $\lambda_{mfp} \sim 100r_L$  we find  $\gamma_{c,rec} \sim 6 \times 10^7$ , again high enough to keep Cen A shining.

We must remember that three important parameters in (16) and (17) are sensitive to local conditions. One is  $\lambda_{\parallel}$ , the length of the reconnection layer. If reconnection is driven by MHD turbulence,  $\lambda_{\parallel}$  is limited above by the coherence length of the turbulence (*e.g.*, Servido *et al* 2011, Zhdankin *et al* 2013). Alternatively, if the radio lobes contain self-organized magnetic structures,  $\lambda_{\parallel}$  will be larger, up to a significant fraction of the domain size (*e.g.*, Benford and Protheroe 2008). A second parameter is the inflow speed,  $v_{in}$ , which is a matter of active current debate. Early work suggested  $v_{in} \ll v_A$  in quiescent systems (*e.g.*, Zweibel and Yamada 2009 and references therein). However, a large body of modern work points to much faster reconnection in collisionless and/or turbulent systems, typically reaching  $v_{in} \gtrsim 0.1v_A$  (*e.g.*, Shay *et al* 2004, Markidis *et al* 2012, Kowal *et al* 2012). Furthermore, large-scale motions in the system can drive reconnection at inflow speeds comparable to the bulk motion speed (*e.g.*, Yamada *et al* 1997; Gekelman *et al* 2012). A third parameter is  $\lambda_{mfp}$ , the scattering mean free path. As with spatial diffusion and shock acceleration,  $\lambda_{mfp}$  must be assumed *ad hoc*, and can vary from Bohm to QL scattering, with orders of magnitude inbetween.

To summarize, the examples here show that reconnection ISR is an attractive alternative to shock acceleration, and has the potential to keep Cen A shining *if local conditions in the reconnection regions are favorable*. However, many details of the physics remain to be worked out before either version of reconnection ISR can be tested robustly against the data.

#### 6.4. Compare the models to the data

The summary of ISR models in this section has mostly been general. How do they compare to the data on Cen A? Key results germane to ISR are as follows.

- *Short lifetimes.* A successful ISR model must be able to energize relativistic electrons rapidly enough to offset radiative losses. For Cen A, the most stringent constraint is the  $\sim 1$  Myr lifetime for  $\gamma \gtrsim 10^6$  electrons observed in  $\gamma$ -rays.
- *Radio spectrum.* The integrated radio spectrum of the outer lobes of Cen A is a power law, with spectral index  $\alpha_{rad} \sim 0.7$ , from  $\sim 10$  MHz to  $\gtrsim 10$  GHz (Alvarez *et al* 2000; H09). The narrowband radio spectrum is relatively constant within the lobes, showing some fluctuations but no large-scale trends (Combi and Romero 1997, McKinley *et al* 2013).\*
- *Gamma-ray spectrum.* The integrated  $\gamma$ -ray spectrum is steeper than the radio spectrum. It has been fit by a power law between  $\sim 200$  MeV to  $\sim 7$  GeV (A10,

<sup>+</sup> Bosch-Ramon (2012) gives an even faster estimate for  $t_{acc}$ , pushing the perpendicular scattering rate close to the Bohm limit. If this is the case,  $\gamma_{c,rec}$  will be even higher than in my illustration here.

\* Problems with incomplete flux recovery make the apparent gradients in the spectral index map based on PAPER data between 123 and 173 MHz (Stefan *et al* 2013) questionable.

Y12), but a slowly curving spectrum also fits the data. The photon statistics are not yet good enough to detect spectral gradients within the lobe.

- *Ratio of  $\gamma$ -ray to radio power.* As discussed in Section 3.1, the observed  $\gamma$ -ray and radio powers require a specific distribution function for relativistic electrons if the source is homogeneous. This constraint is relaxed if the radio and  $\gamma$ -ray emission come from different regions (for instance, the radio from high-B regions and the  $\gamma$ -rays from throughout the lobes).
- *Connection to dynamic models.* An ISR model must make sense in the context of a successful dynamic model. For instance, shock acceleration can only apply if transonic flows exist within the source; reconnection acceleration can apply only if magnetic field reversals exist within the source.

How do the three ISR models fare against these data and constraints?

- *Alfven wave acceleration* is very likely happening in the radio lobes of Cen A. Because Alfven waves are easy to generate and hard to damp, a field of Alfven waves is likely to exist throughout the outer lobes, whether they obey the flow-driven or magnetically-driven models. If the plasma is tenuous enough, Alfvenic ISR can offset radiative losses. However, current models of Alfven wave acceleration are challenged by the broadband, power-law radio spectrum; if Alfvenic ISR is the sole ISR mechanism, more physics is needed. Possible extensions of the models include spatial gradients in the B field and/or the turbulence structure, and a dynamic model of the Alfven wave spectrum.
- *Shock acceleration* will be a key part of the flow-driven models of Section 5.3. If these models apply to Cen A, weak shocks will exist here and there throughout the outer lobes. Standard shock acceleration theory – even allowing for uncertainties in the detailed physics – suggest that even weak shocks can easily maintain a power-law energy spectrum for radio-loud electrons. Thus, if transonic flows exist within the lobes of Cen A, shock acceleration is a very attractive ISR mechanism. Because the shocks will be localized, high-B regions, they probably coexist with Alfvenic ISR operating elsewhere in the radio lobes.
- *Reconnection acceleration* almost certainly exists at some level within the outer lobes of Cen A. On small scales, reconnection is an intrinsic part of MHD turbulence (*e.g.*, Retinò *et al* 2007, Servido *et al* 2011). If Cen A obeys the flow-driven model, small-scale reconnection ISR should be operating throughout the outer lobes, probably augmenting Alfvenic ISR from the same turbulent regions. On large scales, reconnection is essential for the magnetic relaxation involved in magnetic tower models (*e.g.*, Tang and Boozer 2004, Benford and Protheroe 2008). If these models describe Cen A, reconnection ISR may play the major role in maintaining radio emission from the high-B regions, coexisting with Alfvenic ISR operating elsewhere in the source.

### 6.5. Constraints on plasma density

As a final note to this ISR discussion, we must return to Alfvenic ISR. I have argued that this mechanism is operating throughout the lobes of Cen A, no matter which dynamic model holds. However, the condition required for rapid Alfvenic ISR is critical, and possibly contentious. In order for this mechanism to be effective, the Alfven speed must be high,  $v_A = B/(4\pi n_p m_p)^{1/2} \gtrsim 4000 \text{ km s}^{-1}$  (derived in

Section 6.2 under the assumption of a broad-band  $k^{-5/3}$  wave spectrum). If a proton-electron plasma carries the Alfvén waves, this high speed requires a low density,  $n_p \lesssim 3 \times 10^{-7} B_{\mu G}^2 \text{ cm}^{-3}$ , which appears inconsistent with two recent papers (Stawarz *et al* 2013, O’Sullivan *et al* 2013). Both papers suggested much higher densities in the lobes,  $n_p \sim 10^{-4} \text{ cm}^{-3}$ . Such high density, if it exists, would be comparable to that in the surrounding IGM, and would reduce  $v_A$  to  $\sim 200 B_{\mu G} \text{ km s}^{-1}$ , slow enough that Alfvénic acceleration would fail as an ISR mechanism in Cen A. However, the data in both papers are subject to more than one interpretation.

Stawarz *et al* (2013) reported a *tentative* (their italics) detection of diffuse, thermal X-ray emission at  $\sim 0.5 \text{ keV}$  from small regions coincident with the southern radio lobe of Cen A. Assuming this emission comes from plasma within the lobe, they derive a density  $\sim 10^{-4} \text{ cm}^{-3}$ ; but it seems equally likely that this emission is related to the Galactic foreground (for instance part of the large-scale structure detected by ROSAT, shown in Figure 7 of Stawarz *et al*), and/or to the surrounding IGM of the galaxy group in which NGC 5128 resides.

O’Sullivan *et al* (2013) detected a Faraday rotation signal,  $\sim 10 \text{ rad/m}^2$ , apparently associated with inner parts of north and south outer lobes in Cen A. They suggest the Faraday rotation does not come from the IGM of the galaxy group or from a skin associated with the lobe/IGM interface, but rather comes from plasma within the outer lobes. Their particular model (turbulent depolarization on 20-kpc scales and a sub- $\mu G$  B field taken from A10), also requires  $n \sim 10^{-4} \text{ cm}^{-3}$  within the radio lobes.

However, the situation regarding Faraday rotation associated with radio galaxies is complex, and the final story may not yet be known. A large body of previous work has used the lack of detected internal Faraday rotation to place upper limits on thermal gas density with RG lobes (*e.g.*, Spangler and Sakurai 1985, Laing and Bridle 1987, Garrington and Conway 1991; also Feain *et al* 2009 for Cen A). These limits are consistent with the plasma in the lobes being much less dense than surroundings. In addition, as Wykes *et al* (2013) note, the existence of X-ray cavities in galaxy clusters coincident with radio lobes and tails (*e.g.*, Wilson *et al* 2006 for Cyg A, and Wise *et al* 2007 for Hydra A) also points to the plasma density within the lobes being significantly lower than that in the surrounding IGM.

It is possible, of course, that Cen A is the exception to the general rule, and is as dense as its surroundings. But it has long been known that Faraday rotation in many radio galaxies seems to be associated with the immediate surroundings of the radio lobes, either at the lobe/IGM interface or in disturbed IGM close to the radio source (*e.g.*, Dreher *et al* 1987; Rudnick and Blundell 2003; Guidetti *et al* 2011). While this connection is not yet understood – we have no good model of how a Faraday-strong shell forms around the radio lobes – Cen A may be just another example of this effect.

## 7. Discussion and conclusions

In this section I summarize my previous arguments in this paper, discuss which of the models I have proposed might best describe Cen A, and speculate on how these models connect to other evidence we have on the recent history of the galaxy.

### 7.1. Summary I: tentative models for Cen A

In this paper I have shown that the radio galaxy Cen A is on the order of 1 Gyr old; substantially younger models violate observations. Because this is much older than the radiative lifetimes of the relativistic electrons seen in radio and  $\gamma$ -rays, in situ reacceleration (ISR) must be ongoing throughout the 300-kpc-scale radio lobes. I developed the argument in three parts, as follows.

- I showed (in Section 3, also Table 3) that homogeneous, quasi-equipartition ( $u_B \sim u_e$ ) models are *not* required by the data. Inhomogeneous models, in which high-B and low-B regions coexist, are also consistent with the data and probably closer to the real physics. The high-field regions could be shocks within the outer lobes or force-free regions within a large-scale magnetic structure.

- I introduced three toy models to describe the dynamical growth of Cen A (in Section 5, also Tables 4 and 6). (1) The slowest-growing model assumes the outer ends of the radio lobes are driven by *buoyancy*. (2) A second model assumes the radio lobes are magnetically dominated, with large-scale organized structures akin to *magnetic towers*. (3) A third, faster-growing model assumes radio lobe growth is driven by *internal plasma flow*. These models require Cen A to be at least several hundred Myr old, and possibly older than a Gyr. By comparison, the radiative lifetimes range from a few Myr for  $\gamma$ -ray-loud electrons, to at most  $\sim 80$  Myr for radio-loud electrons; thus ISR is needed.

- I explored (in Section 6, also Table 6) three competing ISR models relevant to Cen A. (1) *Alfven wave turbulence* can explain the data if the radio lobe plasma is tenuous and highly variable in time and/or space. (2) *Weak shocks* are an attractive ISR mechanism in the transonic, flow-driven model; they may account for most or all of the radio emission in that model. (3) *Reconnection* is another attractive ISR mechanism, especially in the magnetically driven model, *if* reconnection site physics is consistent with current thinking.

### 7.2. Summary II: which models might work for Cen A?

Having introduced three dynamic models, and explored what ISR mechanism(s) can work within each one, I then compared the models to the data (in Section 5.4 and Section 6.4; also Table 6). While the simplest form of the buoyant model had severe challenges, two models remain viable: flow driven and magnetically driven.

- *Flow-driven models* are the closest to traditional models of FR II sources, and may provide a good description of many tailed FRI sources. Their two-part structure (channel flow plus surrounding cocoon) gives a natural explanation for the transverse spectral structure seen in Cen A. If the channel flow is transonic, the internal shocks it drives are an attractive way to explain the radio filaments and radio spectrum of Cen A.
- *Magnetically driven models*, while less popular in the radio galaxy literature, are an intriguing alternative to flow-driven models. The large-scale, self-organized structures inherent in these models are a tempting explanation for the large structures and gradients seen in total and polarized radio emission. If these models describe Cen A, large-scale reconnection sites probably supplement Alfvénic ISR throughout the lobes.

However, neither of these models has been developed to the point where it can confidently be said to describe Cen A. Until my suggested scenarios in this paper



are supported by dedicated modelling and/or simulations, they remain no more than speculations. While the internal physics of competing ISR mechanisms clearly needs further work, the most immediate – and addressible – test of each model is under what conditions it can explain the large-scale structure of Cen A.

Flow-driven models are perhaps most challenged by the lack of brightening at the outer ends of the lobes, where the channel flow should be decelerating and/or developing terminal shocks. I have speculated that lower Mach number flows will not suffer such problems, but – because most work on flow-driven models has considered high Mach number flows – it is not yet clear under what conditions, if at all, models driven by slower flows can avoid disruptive instabilities and create large-scale radio lobes resembling those in Cen A.

Magnetically-driven models are perhaps most challenged by the lack of large, synchrotron-faint internal cavities as predicted by existing models. I have suggested that the radio lobes may contain more complex, self-organized magnetic structures, but this remains to be demonstrated. Work is especially needed to learn whether AGN-driven plasmas can access the necessary high-order magnetic modes in a soft-boundary system (such as a radio lobe in the IGM), and whether the plasma/field mix inside such systems is sufficiently radio-loud to create radio lobes resembling those in Cen A.

### 7.3. Connect to the recent history of the galaxy

To close, some possible connections between Cen A and recent events in the history of its parent galaxy deserve mention.

*Very recent history: disrupted jets?* Although active jets from the AGN are feeding the kpc-scale inner radio lobes, no detectable jets connect the inner lobes to the outer lobes on either side of the AGN (Neff *et al* 2014). If ongoing energy transport requires a detectable jet, then both outer lobes are disconnected from their engine. Are they dying? If so, how quickly will they fade from view?

Because the radio- and  $\gamma$ -ray-loud electrons require frequent ISR in order to keep shining, we must ask, on what timescale the ISR will cease if energy flow to the radio lobes is disrupted. Turbulence is the common denominator in all three ISR mechanisms. It is clearly required for Alfvén-wave ISR, and it is implicated in our two alternative ISR models. Thus, the lobes will fade when the turbulence decays.

We know that nondriven fluid turbulence will decay in no more than several turnover times,  $\tau_t = \lambda_t/v_t$  (where  $\lambda_t$  and  $v_t$  are the characteristic scale and velocity of the turbulence). We can estimate  $\lambda_t \sim \lambda_{max} \sim 30$  kpc from the images, but we have no direct probe of  $v_t$ . The flow-driven model allows a possible *ansatz*: if the field is maintained by a turbulent dynamo,  $B^2/4\pi \lesssim \rho v_t^2$ , and thus  $v_t \gtrsim v_A$ . Alternatively, with the magnetically driven model we can directly take  $v_A$  as the turbulent turnover speed. Thus, our limit  $v_A \gtrsim 4000$  km/s (from Section 6.2) suggests  $\tau_t \lesssim 8$  Myr. We therefore expect turbulence in the outer lobes to decay in no more than  $\sim 30$  Myr. This is longer than the lifetime of the  $\gamma$ -ray-loud electrons, and comparable to the lifetime of the radio-loud electrons; the lobes will fade quickly if the turbulence stops being driven.

It follows that, if the outer lobes are disconnected from the AGN right now, this situation cannot have lasted long. Whatever disrupted the energy flow from the AGN must have happened no more than a few tens of Myr ago. Did the AGN go through

a quiescent period, for the past few tens of Myr, and then revive itself only a few Myr ago? If so, was this part of a regular duty cycle, or is it evidence of an unusual disruptive event in the galaxy's recent history?

*Previous history: did a merger launch the radio galaxy?* We have seen that Cen A is on the order of a Gyr old. It is interesting to compare this age range to the dynamic history of NGC 5128. The evidence suggests that at least two significant events – encounters or mergers – have happened to this galaxy in the past few Gyr.

One line of evidence comes from the dramatic gas/dust disk in the core of NGC5128. Because it is warped and twisted we must be seeing it fairly soon after its formation, as it settles into a stable state within the galaxy's gravitational potential. The exact rate at which the disk settles depends on details of the galaxy's structure. If the galaxy is prolate, models suggest the disk is only  $\sim 200$  Myr old (Quillen *et al* 1993); if the galaxy is oblate, the disk is  $\sim 700$  Myr old (Sparke 1996). If, as generally assumed, the disk has been left behind by a recent merger, that event happened less than a Gyr ago.

Another line of evidence comes from the galaxy's stars; NGC5128 has a complex star formation history. While the bulk of the stars are at least 10 Gyr old, recent work has found a younger population, which may be as young as  $\sim 2-3$  Gyr (*e.g.*, integrated light spectroscopy of globular clusters, Woodley *et al* 2010; resolved studies of halo stars, Rejkuba *et al* 2011). If this recent burst of star formation was triggered by an encounter or merger, that event happened  $\sim 2-3$  Gyr ago.

While we do not know what initiates an activity cycle in an AGN, the ages of these two recent events are intriguing. The (relatively young) age of the disk and the (somewhat older) age of the young stellar population in NGC5128 bracket the ages that the dynamic models predict for the outer lobes. Did one of these recent encounters also trigger AGN activity and create the radio galaxy Cen A?

## Acknowledgments

It is a pleasure to thank Susan Neff, Frazer Owen, Sarka Wykes, Hui Li and Martin Hardcastle for many illuminating conversations about radio galaxy physics in general, and Cen A in particular. Insightful comments from the referees contributed significantly to this paper. Norbert Junkes kindly provided his Parkes image of Cen A. This research made use of the NASA/IPAC Extragalactic Database (NED) which is operated by the Jet Propulsion Laboratory, California Institute of Technology, under contract with the National Aeronautics and Space Administration. The National Radio Astronomy Observatory is a facility of the National Science Foundation operated under cooperative agreement by Associated Universities Inc.

## Appendix A. Electron radiative lifetimes

If we do not know the historical magnetic field through which an electron has propagated, we cannot uniquely determine its age. In this Appendix I set up limiting cases which can be useful in the absence of such historical knowledge.

The basic equations (1) and (4) (in Section 3.1) for radiative losses by a single particle, due to synchrotron radiation and inverse Compton scattering (ICS), allow a

useful definition of the particle's radiative lifetime,  $t_{rad}$ :

$$A\gamma \int_0^{t_{rad}} (u_{rad}(t) + u_B(t)) dt \simeq A\gamma \langle u_{rad} + u_B \rangle t_{rad} = 1 \quad (\text{A.1})$$

Here,  $A = (4/3)c\sigma_T$ ,  $u_{rad}$  and  $u_B$  are the energy densities in local radiation and magnetic fields, and the angle brackets define the time-averaged radiation and magnetic fields seen by the particle historically.

For ICS, we know the particle  $\gamma$  directly, and we can write (A.1) as

$$t_{ICS}(\gamma) = \frac{1}{A\gamma \langle u_{rad} + u_B \rangle} \quad (\text{A.2})$$

In many applications  $u_{rad}$  is that of the CMB and does not vary with time. In this case, the longest possible life for an ICS electron happens when  $u_B \ll u_{CMB}$  throughout the particle's life, giving

$$t_{ICS}^{max}(\gamma) = \frac{1}{A\gamma \langle u_{CMB} \rangle} \simeq \frac{2.3 \times 10^6}{\gamma} \text{ Myr} \quad (\text{A.3})$$

However, for synchrotron radiation at a given  $\nu_{obs}$ , we only know the particle  $\gamma$  as a function of the magnetic field *in which the particle now radiates*,  $B_{now}$ :  $\nu_{obs} = a\gamma^2 B_{now}$ . The equivalent to (A.2) is

$$t_{sy}(\nu_{obs}) = \left( \frac{a}{\nu_{obs}} \right)^{1/2} \frac{B_{now}^{1/2}}{A \langle u_{CMB} + u_B \rangle} \quad (\text{A.4})$$

In this situation we can again find a limiting case by assuming  $u_B \ll u_{CMB}$  throughout the particle's life:

$$t_{sy}^{max}(\nu_{obs}) = \left( \frac{a}{\nu_{obs}} \right)^{1/2} \frac{8\pi B_{now}^{1/2}}{A \langle B_{CMB}^2 \rangle} \simeq 57 \frac{B_{now, \mu G}^{1/2}}{\nu_{GHz}^{1/2}} \text{ Myr} \quad (\text{A.5})$$

## Appendix B. Momentum-driven growth of a radio lobe

In this appendix I set up a simple model of flow-driven growth for the outer lobes (or tails) of an FRI radio source such as Cen A. The model is motivated by successful models of FRII sources, and also by observations (*e.g.*, Katz-Stone & Rudnick 1996, Katz-Stone *et al* 1999) which reveal complex spectral structure within the tails of some FRI sources. Consider a two-part radio lobe or tail: energy and momentum is carried along a central channel, with radius  $r_c$ , cross-section  $A_c = \pi r_c^2$ , density  $\rho_c$  and speed  $v_c$ . The channel is surrounded by a larger and nearly static cocoon with radius  $a$ , which we observe as the radio lobe. Both lobe and channel have length  $D$ . The channel, the cocoon and the ambient IGM are all in pressure balance at some pressure  $p$ . All flows are subrelativistic and have no more than a dynamically small magnetic field.

*Growth rate of the lobe.* The front end of the channel, which is also the front end of the lobe, advances into the IGM at speed  $v_{end} = dD/dt$ . The advance rate depends on the area,  $A_{end}$ , over which the momentum flux from the channel is spread when it reaches the contact surface between the lobe and the IGM. Momentum conservation in the frame of the contact surface gives

$$\rho_c (v_c - v_{end})^2 + p = (\rho_{IGM} v_{end}^2 + p) \frac{A_{end}}{A_c} \quad (\text{B.1})$$

(e.g., Norman *et al* 1983, or Mizuta *et al* 2004). It is easy to show from this relation that  $v_{end} \ll v_c$  if  $\rho_c \ll \rho_{IGM}$ ; thus

$$\rho_c v_c^2 + p \simeq (\rho_{IGM} v_{end}^2 + p) \frac{A_{end}}{A_c} \quad (\text{B.2})$$

This expression can be rewritten in terms of the Mach numbers<sup>‡</sup>, as

$$\Gamma_c \mathcal{M}_c^2 = \Gamma_{IGM} \mathcal{M}_{end}^2 \frac{A_{end}}{A_c} + \left( \frac{A_{end}}{A_c} - 1 \right) \quad (\text{B.3})$$

Unfortunately, the area  $A_{end}$  is not well specified by current models or data. It may be as small as the cross section of the channel,  $A_c$ , or it may be larger, up to the full cross section of the lobe,  $\pi a^2$ . We thus have useful inequalities:

$$\rho_c v_c^2 \gtrsim \rho_{IGM} v_{end}^2 ; \quad \Gamma_c \mathcal{M}_c^2 \gtrsim \Gamma_{IGM} \mathcal{M}_{end}^2 \quad (\text{B.4})$$

The lower limits are reached when  $A_{end} \rightarrow A_c$ .

*Power needed to grow the lobe.* Energy usage in the lobe depends on the evolution of its geometry as it grows, which is also not well specified by models or data. In one extreme case, the lobe radius may stay constant while the outer end advances. Alternatively, and perhaps more likely, the lobe may grow self-similarly, keeping the ratios  $r_c/a$  and  $a/D$  constant. I parameterize this uncertainty as  $dV/dt = 3\pi a^2 f_V v_{end}$ , where  $f_V \in (1, 3)$  describes the range from constant-radius growth to self-similar growth.

The power carried in the channel flow is

$$P_c = \pi r_c^2 v_c \left[ \frac{\Gamma_c p}{\Gamma_c - 1} + \frac{1}{2} \rho_c v_c^2 \right] \quad (\text{B.5})$$

Our goal is to write  $P_c$  in terms of known quantities. To do this, we can use the fact that the power supplied to an outer lobe must balance the growth rate of total energy in an outer lobe,  $U_{OL}$  (including kinetic energy in the channel and work done on IGM). Collecting all terms gives

$$\frac{dU_{OL}}{dt} = \pi a^2 f_V v_{end} \left( \frac{\Gamma_c p}{\Gamma_c - 1} \right) + \frac{1}{2} \pi r_c^2 f_V v_{end} \rho_c v_c^2 \left( 1 + 2 \frac{A_{end}}{A_c} \right) \quad (\text{B.6})$$

The first term represents the enthalpy budget of the expanding lobe, and assumes the adiabatic index is the same for the channel and the cocoon. The second term describes the kinetic energy of, and work done by, the channel flow. I have assumed the channel expands proportionally to the full lobe ( $r_c/a$  remains constant) and that the channel flow does work over an area  $A_{end}$ .

To proceed, equating  $P_c = dU_{OL}/dt$ , and using (B.3) to write the  $\rho_c v_c^2$  term in (B.6) in terms of known quantities, gives

$$P_c = \pi a^2 f_V v_{end} \frac{\Gamma_c p}{\Gamma_c - 1} (1 + \mathcal{C}) \quad (\text{B.7})$$

Here, the first term is the basic power needed to grow the lobe against the IGM pressure, and the additional term

$$\mathcal{C} = \frac{r_c^2}{a^2} \frac{\Gamma_c - 1}{2\Gamma_c} \left( 1 + \frac{2A_{end}}{A_c} \right) \left[ \Gamma_{IGM} \mathcal{M}_{end}^2 \frac{A_{end}}{A_c} + \left( \frac{A_{end}}{A_c} - 1 \right) \right] \quad (\text{B.8})$$

<sup>‡</sup> The internal Mach number of the core is  $\mathcal{M}_c = v_c/c_{s,c}$ ; the Mach number of the end relative to the IGM is  $\mathcal{M}_{end} = v_{end}/c_{s,IGM}$ .

is the extra power needed to maintain the channel. When  $A_{end} \rightarrow A_c$ , the expression for  $P_c$  in (B.7) reaches its lowest value. Thus, in general we have

$$P_c \gtrsim \pi a^2 f_V v_{end} \frac{\Gamma_c p}{\Gamma_c - 1} \left[ 1 + \frac{3r_c^2}{a^2} \frac{\Gamma_c - 1}{2\Gamma_c} \Gamma_{IGM} \mathcal{M}_{end}^2 \right] \quad (\text{B.9})$$

Because  $p$  and  $a$  are known from the data, (B.9) shows that the minimum power  $P_c$  required for a specific choice of  $v_{end}$  (and therefore  $\mathcal{M}_{end}$ ) depends only on the fractional channel radius,  $r_c/a$  and the volume growth factor  $f_V$ . Some numerical examples are discussed in the text and given in Table 5.

## References

- Abdo A A *et al* (Fermi-LAT Collaboration) 2010 *Science* **328** 725 (A10)  
 Alvarez H, Aparici J, May J and Reich P, 2000 *Astron. Astrophys.* **355** 863  
 Benford G and Protheroe R, 2008 *Mon. Not. R. Astron. Soc.* **383** 663  
 Bicknell G 1984 *Astrophys. J.* **286** 68  
 Bicknell G and Melrose, D 1982 *Astrophys. J.* **262** 511  
 Borovsky J and Eilek J 1986 *Astrophys. J.* **308** 929  
 Bouchard A, Jerjen H, Da Costa G S and Ott J 2007 *Astron. J.* **133** 261  
 Bosch-Ramin V 2012 *Astron. Astrophys.* **542** 125  
 Brunetti G, Blasi P, Cassano R. and Gabici S 2004 *Mon. Not. R. Astron. Soc.* **350** 1174  
 Burbidge G 1956 *Astrophys. J.* **124** 416  
 Burn B J 1966, *Mon. Not. R. Astron. Soc.* **133** 67  
 Casse F, Lemoine M and Pelletier G 2002 *Phys. Rev. D* **65** 023002  
 Combi J and Romero G 1997 *Astron. Astrophys. Supp.* **121** 11  
 Croston J H, Kraft R P, Hardcastle M J *et al* 2009 *Mon. Not. R. Astron. Soc.* **395** 1999  
 de Gouveia dal Pino E M and Lazarian A 2005 *Astron. Astrophys.* **441** 845  
 De Young D S 1986 *Astrophys. J.* **307** 62  
 Doe S M, Ledlow M J, Burns J O and White R A 1995 *Astron. J.* **110** 46  
 Dosch A, Shalcky A and Tautz R C 2011 *Mon. Not. R. Astron. Soc.* **413** 2950  
 Dreher J W, Carilli C L and Perley R A 1987 *Astrophys. J.* **316** 611  
 Drury L O'C 1983 *Reports in Progress in Physics* **46** 973  
 Drury L O'C 2012 *Mon. Not. R. Astron. Soc.* **422** 2474  
 Eilek J 1979 *Astrophys. J.* **230** 373  
 Eilek J and Arendt P 1996 *Astrophys. J.* **457** 150  
 Feain I J, Ekers R D, Murphy T *et al* 2009 *Astrophys. J.* **707** 114  
 Feain I J, Cornwell T, Ekers R *et al* 2011 *Astrophys. J.* **740** 17  
 Finoguenov A, Davis D S, Zimer M and Mulchaey J S 2006 *Astrophys. J.* **646** 143  
 Garrington S T and Conway R G 1991 *Mon. Not. R. Astron. Soc.* **250** 198  
 Geckelman W, Lawrence E and Van Compernelle B 2012 *Astrophys. J.* **753** 131  
 Giacalone J 2005 *Astrophys. J.* **624** 765  
 Gourgouliatos K N and Lyutikov M 2012 *Mon. Not. R. Astron. Soc.* **420** 505  
 Guidetti D, Laing R A, Bridle A H, *et al* 2011 *Mon. Not. R. Astron. Soc.* **413** 2525  
 Gunn J E and Gott J R III 1972 *Astrophys. J.* **176** 1  
 Hardcastle M, Cheung C, Feain I and Stawarz L 2009 *Mon. Not. R. Astron. Soc.* **393** 1041 (H09)  
 Harris G L H, Rejkuba M and Harris W E 2010 *Pub. Astron. Soc. Pacific* **27** 457  
 Haugen N E, Brandenburg A and Dobler W 2004 *Phys. Rev. E* **70** 016308  
 Junkes N, Haynes F, Jarnett J and Jauncey D 1993 *Astron. Astrophys.* **269** 29  
 Kagan D, Milosavljevic M and Spitkovsky A 2013 *Astrophys. J.* **774** 41  
 Kang H 2011 *J. Kor. Astron. Soc.* **44** 49  
 Katz-Stone D M and Rudnick L 1996 *Astrophys. J.* **448** 146  
 Katz-Stone D M, Rudnick L, Butenhogg C and O'Donoghue A A 1999 *Astrophys. J.* **516** 716  
 Kowal G, de Gouveia Dal Pino E and Lazarian A 2012 *Phys. Rev. Letters* **108** 241102  
 Krachentsev I D, Tully, R B, Dolphin A, *et al* 2007 *Astron. J.* **133** 504  
 Kraft R P, Forman W R, Hardcastle M J, *et al* 2009 *Astrophys. J.* **698** 2036  
 Lacombe, C 1977 *Astron. Astrophys.* **54** 1  
 Laing R A and Bridle A H 1987 *Mon. Not. R. Astron. Soc.* **228** 557  
 Li H, Lovelace R, Finn J and Colgate S 2001 *Astrophys. J.* **561** 915  
 Litvinenko Y E 1999 *Astron. Astrophys.* **685** 690

- Lynden-Bell D 1996 *Mon. Not. R. Astron. Soc.* **279** 389
- Markidis S, Henri P, Lapenta G *et al* 2012 *Nonlin. Processes Geophys.* **18** 145
- McKinley B, Briggs F, Gaensler B *et al* 2013 *Mon. Not. R. Astron. Soc.* in press
- Mizuta A, Yamada S and Takabe H 2004, *Astrophys. J.* **606** 804
- Molina F Z, Glover S C O, Federrath C and Klessen R S 2012 *Mon. Not. R. Astron. Soc.* **423** 2680
- Morganti R, Killeen N E B, Ekers R D and Osterloo T A 1999 *Mon. Not. R. Astron. Soc.* **307** 750
- Myers S T and Spangler S R 1985 *Astrophys. J.* **291** 52
- Nakamura M, Li H and Li S 2006 *Astrophys. J.* **652** 2006
- Neff S, Eilek J and Owen F 2014 in preparation
- Norman M L, Winkler K-H and Smarr, L, 1983, in *Astrophysical Jets* (eds A Ferrari and A G Pacholczyk; Dordrecht: Reidel) 227;
- O'Sullivan S, Reville B and Taylor A M 2009 *Mon. Not. R. Astron. Soc.* **400** 2480
- O'Sullivan S P, Feain I J, McClure-Griffiths N M, *et al* 2013 *Astrophys. J.* **764** 162
- Pacholczyk A G. 1970 *Radio Astrophysics* (San Francisco: Freeman)
- Quillen A C, Graham J R and Frogel J A 1993 *Astrophys. J.* **412** 550
- Rejkuba M, Harris W E, Greggio L and Harris G L H 2011 *Astron. Astrophys.* **526** 123
- Retinò A, Sundkvist D, Viavads A, *et al* 2011 *Nature Physics* **3**, 236
- Riquelme M A and Spitkovsky A 2010 *Astrophys. J.* **717** 1054
- Romanova M M and Lovelace R V E 1992 *Astron. Astrophys.* **262** 26
- Rudnick L and Blundell K M 2003 *Astrophys. J.* **588** 143
- Schekochihin A A, Cowley S C, Taylor S F, *et al* 2004 *Astrophys. J.* **612** 276
- Schure K M, Bell A R, Drury L O'C and Bykov A M 2012 *Space. Sci. Rev.* **173** 491
- Servidio S, Dmitruk P, Crego A, *et al* 2011 *Nonlin. Processes Geophys.* **18** 675
- Shay M A, Drake J F, Swisdak M and Rogers B N 2005 *Phys. Plasmas*. **11** 2199
- Spangler, S R and Sakurai T 1985 *Astrophys. J.* **297** 84
- Sparke L S 1996 *Astrophys. J.* **473** 810
- Stawarz L and Petrosian V 2008 *Astrophys. J.* **681** 1725
- Stawarz L, Tanaka Y T, Madejsk, G *et al* 2013 *Astrophys. J.* **766** 48
- Stefan I I, Carilli C L, Green D A, *et al* 2013 *Mon. Not. R. Astron. Soc.* in press.
- Sun M, Voit G M, Donahue, M, *et al* 2009, *Astrophys. J.* **693** 1142
- Tang X Z 2008 *Astrophys. J.* **679** 1000
- Tang X Z and Boozer A H 2004 *Phys Plasmas* **11** 2679
- Tregillis I L, Jones T W and Ryu D 2001 *Astrophys. J.* **557** 475
- Uzdensky D A and MacFadyen A I 2006, *Astrophys. J.* **647** 1192
- Wilson A S, Smith D A and Young A J 2006 *Astrophys. J.* **644** L9
- Wise M W, McNamara B R, Nulsen P E J *et al* 2007 *Astrophys. J.* **659** 1153
- Woodley K A, Harris W E, Puzia T H *et al* 2010 *Astrophys. J.* **708** 1335
- Wykes S, Croston J, Hardcastle M *et al* 2013 *Astron. Astrophys.* **558** A19
- Yamada M, Ji H, Hsu S *et al* 1997 *Phys. Plasmas* **4** 1936
- Yang R-Z, Sahakyan N, de Ona Wilhelmi E, *et al* 2012 *Astron. Astrophys.* **542** A19 (Y12)
- Zhdankin V, Uzdensky D A, Perez J C and Boldyrev S, 2013 *Astrophys. J.* **771** 124
- Zhou Y, Matthaeus W and Dmitruk P, 2004 *Rev. Mod. Phys* **76** 1015
- Zweibel E G and Yamada M 2009 *Ann. Rev. Astron. Astrophys.* **47** 129